



OPEN ACCESS

EDITED BY

Matthias Haeckel,
Helmholtz Association of German
Research Centres (HZ), Germany

REVIEWED BY

Thomas G. Dahlgren,
Norwegian Research Institute (NORCE),
Norway

Andrew John Gooday,
National Oceanography Centre,
Southampton, United Kingdom

*CORRESPONDENCE

Tanja Stratmann

✉ tanja.stratmann@nioz.nl

RECEIVED 26 January 2023

ACCEPTED 19 April 2023

PUBLISHED 12 May 2023

CITATION

Stratmann T (2023) Role of polymetallic-nodule dependent fauna on carbon cycling in the eastern Clarion-Clipperton Fracture Zone (Pacific).

Front. Mar. Sci. 10:1151442.

doi: 10.3389/fmars.2023.1151442

COPYRIGHT

© 2023 Stratmann. This is an open-access article distributed under the terms of the [Creative Commons Attribution License \(CC BY\)](https://creativecommons.org/licenses/by/4.0/). The use, distribution or reproduction in other forums is permitted, provided the original author(s) and the copyright owner(s) are credited and that the original publication in this journal is cited, in accordance with accepted academic practice. No use, distribution or reproduction is permitted which does not comply with these terms.

Role of polymetallic-nodule dependent fauna on carbon cycling in the eastern Clarion-Clipperton Fracture Zone (Pacific)

Tanja Stratmann^{1,2*}

¹Department of Earth Sciences, Utrecht University, Utrecht, Netherlands, ²Department of Ocean Systems, NIOZ Royal Netherlands Institute for Sea Research, 't Horntje (Texel), Netherlands

The abyssal seafloor in the Clarion-Clipperton Fracture Zone (CCZ) in the central Pacific is covered with large densities of polymetallic nodules, i.e., metal concretions containing iron, manganese, nickel, cobalt, and copper. Nodules are of economic importance for these metals, but they also host a variety of deep-sea fauna. In a recent study it was estimated that the removal of these nodules would lead to a loss of up to 18% of all taxa in the CCZ. Here, I assess the impact of removing these nodule-dependent taxa on carbon cycling at two sites (B4S03, B6S02) of the Belgian exploration license area in the eastern CCZ. For this purpose, I developed two highly resolved carbon-based food web models with 71 (B6S02) to 75 (B4S03) food-web compartments consisting of different detritus pools, bacteria, metazoan meiobenthos, macrobenthic isopods, polychaetes and other macrobenthos, megabenthic cnidarians, crustaceans, poriferans, holothurians and other invertebrate megabenthos, and fish. These compartments were connected with 303 (B6S02) to 336 (B4S03) links which were reduced by 5–9% when nodule-dependent faunal compartments were removed. The models estimated the “total system throughput” $T_{..}$ i.e., the sum of all carbon flows in the food webs, in intact food webs as $1.18 \text{ mmol C m}^{-2} \text{ d}^{-1}$ and $1.20 \text{ mmol C m}^{-2} \text{ d}^{-1}$ at B4S03 and B6S02, respectively, whereby 69.8% (B6S02) to 71.2% (B4S03) of $T_{..}$ flowed through the microbial loop. A removal of the nodule-dependent fauna did not affect this microbial loop but reduced the scavenger loop by 56.5% (B6S02) to 71.6% (B4S03). Overall, nodule-dependent fauna is responsible for only a small fraction of total carbon cycling at the eastern CCZ. Therefore, when the effect of prospective deep-seabed mining on carbon cycling is investigated, its impact on benthic prokaryotes and the microbial loop should be addressed specifically.

KEYWORDS

abyssal plains, linear inverse model, ferromanganese nodules, network indices, food-web model

1 Introduction

The abyss between 3,000 and 6,000 m water depth is the largest ecosystem on our planet (Gage and Tyler, 1991) and covers 85% of the seafloor (Harris et al., 2014). It consists of abyssal hills, abyssal mountains, and abyssal plains. The latter can have a difference in elevation between hilltops and valleys of 0 to 300 m and are often very flat with slopes of less than 0.05° (Cormier and Sloan, 2018). Abyssal plains are subdivided by mid-ocean ridges, like the East-Pacific Rise, deep-sea trenches, and island arcs, and interspersed with hills and mountains (Smith et al., 2008).

Abyssal plains are covered with polymetallic nodules in areas with well oxygenated bottom waters, sedimentation rates of less than 20 mm kyr⁻¹, and high numbers of shark teeth, shells of plankton, or small rocks at the sediment surface that can act as nuclei for these nodules (Hein et al., 2013; Hein and Koschinsky, 2014; Petersen et al., 2016). The nodules are concretions of iron oxide-hydroxide and manganese oxide (Hein and Koschinsky, 2014) and contain nickel, copper, cobalt, titanium, molybdenum, lithium, rare earth elements, and yttrium (Petersen et al., 2016). They form with growth rates of 1 to 10 mm million yr⁻¹ (Petersen et al., 2016). Due to their high content of metals that are currently in demand for the transition from a fossil fuel-based economy to a renewable-energy based economy, polymetallic nodules are considered a potential future source of cobalt, copper, nickel, and rare earth elements (Hein et al., 2013).

Areas with polymetallic nodule densities of economic interest are the Central Indian Ocean Basin, the seabed around the Cook Islands, and the Clarion-Clipperton Fracture Zone (CCZ) (Kuhn et al., 2017). The CCZ is located south of Hawaii and west of Mexico in the central Pacific Ocean between 0°N , 160°W and 23.5°N , 115°W (International Seabed Authority, 2011). It has very variable nodule densities between on average $\sim 1.5\text{--}3\text{ kg m}^{-2}$ in the south to on average $\sim 7.5\text{ kg m}^{-2}$ in the east (Washburn et al., 2021) and experiences a north-west ($1.3\text{ mg C}_{\text{org}}\text{ m}^{-2}\text{ d}^{-1}$) to south-east ($1.8\text{ mg C}_{\text{org}}\text{ m}^{-2}\text{ d}^{-1}$) gradient in particulate organic carbon flux (Vanreusel et al., 2016). These two environmental variables together with seafloor topography drive the different habitat classes in the CCZ (McQuaid et al., 2020).

Polymetallic nodules are not only interesting from an economic point of view, but also provide essential hard substrate for deep-sea benthos: Stalked sponges, such as *Hyalonema (Cyliconemaoida) ovuliferum* (Kersken et al., 2018), the encrusting sponge *Plenaster craigi* (Lim et al., 2017), and large xenophyophores (Gooday et al., 2017) grow on them. In fact, Veillette et al. (2007) identified 73 protozoan and 17 metazoan taxa, mainly of macrofaunal size, attached to polymetallic nodules from the CCZ. This nodule epibenthos includes a variety of taxa, e.g., polychaetes, bryozoans, crustaceans, molluscs, and foraminiferans (Mullineaux, 1987; Gooday et al., 2015), of which more than half are suspension or deposit feeders (Mullineaux, 1989). Furthermore, Vanreusel et al. (2016) showed that even mobile benthos might benefit from the presence of nodules as their densities were higher in areas with nodules compared to nodule-free areas. To quantify the role of polymetallic nodules for trophic and non-trophic interactions in the CCZ, Stratmann et al. (2021) recently presented a highly resolved interaction-web model. When the authors removed the nodules

from the interaction web, they detected knock-down effects causing the loss of 17.9% of all taxa and 30.6% of all network links. Their detailed model estimated that 4% of all meiobenthos (i.e., benthos $>32\text{ }\mu\text{m}$), 50% of the macrobenthos (i.e., benthos $>250\text{ }\mu\text{m}/500\text{ }\mu\text{m}$), 45% of the invertebrate megabenthos (benthos $>1\text{ cm}$), and 0.5% of the fish were missing and the most impacted phyla were Bryozoa, Cnidaria, Platyhelminthes, and Porifera. Several of the taxa affected by nodule removal in the CCZ as modelled by Stratmann et al. (2021) occur in the exploration license area of the Belgian company *Global Sea Mineral Resources* (GSR) in the eastern CCZ (Supplementary Table 1). Therefore, by evaluating which of the taxa that disappeared due to the modelled knock-down effects are part of the present food-web model (short summary is presented in Supplementary Table 1), and by subsequently excluding these from the model, one should be able to assess the impacts of polymetallic nodule removal on carbon cycling.

Short-term carbon cycling in the abyss is dominated by prokaryotes (Stratmann et al., 2018b; Sweetman et al., 2019), with the contribution of macrobenthos to phytodetritus cycling increasing after several days (Witte et al., 2003). In fact, carbon-based food-web models for deep-sea stations in the NE Atlantic, the NE Pacific, and the SE Pacific estimated that prokaryotes contribute $>70\%$ to total benthic respiration at these specific sites (van Oevelen et al., 2012; Dunlop et al., 2016; Durden et al., 2017; de Jonge et al., 2020). These carbon-based food web models are based on the principle of mass conservation and combine physiological parameters (e.g., assimilation and growth efficiency, secondary production, mortality, respiration), with site-specific flux constraints on carbon influx and loss, and biomasses of individual food-web compartments to calculate the carbon flows between compartments in the pre-defined topological food-web (Soetaert and van Oevelen, 2009; van Oevelen et al., 2010). They have been used previously to assess the potential recovery from a small-scale sediment disturbance in the SE Pacific (Stratmann et al., 2018a; de Jonge et al., 2020) and here, they will be applied to estimate changes in carbon flows depending on the presence and absence of nodule-dependent fauna at two sites of the GSR exploration license area in the CCZ.

I will assess (1) the potential small-scale variability in carbon cycling between two sites in the north-eastern CCZ that lay approximately 280 km apart, and (2) the potential reduction in total carbon cycling that the removal of nodule-dependent fauna from the abyssal food web might cause.

2 Materials and methods

2.1 Study site

In the north-eastern CCZ, the GSR exploration license area stretches from 16°N , -128°E to 13°N , -122°E and includes three non-adjacent areas, the so-called B2, B4, and B6 areas (Figure 1). The most western area B2 is located at $\sim 15^\circ 43'\text{ N}$, $-126^\circ 42'\text{ E}$, the central area B4 is located at $\sim 14^\circ 6'\text{ N}$, $-125^\circ 52'\text{ E}$, and the most eastern area B6 is located at $\sim 13^\circ 51'\text{ N}$, $-123^\circ 17'\text{ E}$. Inside the B4 and B6 areas, two $10\times 20\text{ km}$ sampling sites, the B4S03 (14.112°N ,

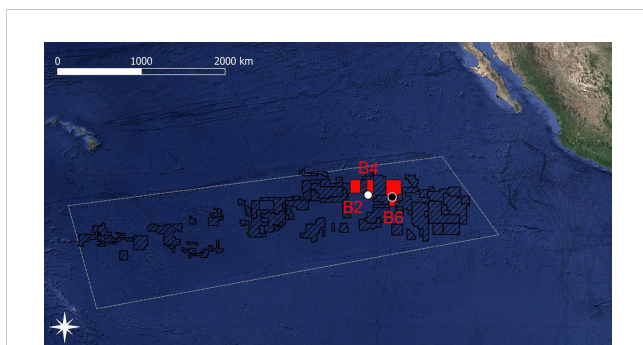


FIGURE 1

Map of the exploration license areas (black dashed areas) within the Clarion-Clipperton Fracture Zone (white dashed polygon based on the working definition of the CCZ by Glover et al. (2015)). The Global Sea Mineral Resources (GSR) exploration license areas are shown in red and the sites B4S03 and B6S02 are indicated by white and black dots, respectively. Copyright for shapefile for the exploration license areas within the CCZ area: © International Seabed Authority 2007-2020.

-125.871°E) and B6S02 (13.894°N, -123.297°E) sites, were identified by de Smet et al., (2017) based on differences in polymetallic nodule properties.

Water depth at the two sites ranges between 4,470 and 4,560 m and the sediment is mainly muddy (mud content: 88.7–91.5%, sand content: 11.3–8.5%) with a median grain size of 16.5–18.5 μm (de Smet et al., 2017). Nodule density is $22.2 \pm 2.41 \text{ kg m}^{-2}$ (\pm standard error) at B4S03 and $27.3 \pm 0.62 \text{ kg m}^{-2}$ at B6S02 with a nodule surface coverage of $36.2 \pm 2.95\%$ and $31.1 \pm 8.43\%$, respectively, and a nodule volume of $92.6 \pm 6.95 \text{ cm}^3$ and $69.7 \pm 13.7 \text{ cm}^3$ (de Smet et al., 2017).

2.2 Food-web structure

Food webs in the GSR exploration license area consisted of the abiotic compartments detritus (phytodetritus, semi-labile detritus, refractory detritus), dissolved organic carbon (DOC), and carrion, and the biotic compartments bacteria, metazoan meiobenthos (4 compartments), macrobenthos (39 compartments), invertebrate megabenthos (25 compartments), and fish (3 compartments). Metazoan meiobenthos and macrobenthic isopods were divided in feeding types based on peer-reviewed literature (Supplementary Tables 2, 3). The food-web compartments of all other macrobenthos, invertebrate megabenthos, and fish compartments resembled the highest taxonomic resolution possible, i.e., family level for macrobenthic polychaetes, (mainly) class level for arthropods, and phyla and class level for all other fauna.

Metazoan meiobenthos ($>32 \mu\text{m}$) included copepods and crustacean nauplii (Pape et al., 2017) that both deposit-feed on bacteria, phytodetritus, and semi-labile detritus (Supplementary Table 2). Nematodes were classified as epistrate feeders, selective, and non-selective deposit feeders following Wieser (1953) based on the nematode genera present in the GSR exploration license area (Pape et al., 2017). They feed on bacteria, phytodetritus, and semi-labile detritus (Supplementary Table 2).

Macrobenthos ($>300 \mu\text{m}$) contained annelids, arthropods, molluscs, brachiopods, nematodes, nemerteans, echinoderms, and sipunculans (de Smet et al., 2017), that were identified to be carnivorous, (non-selective or subsurface) deposit feeders, filter- and suspension feeders, scavengers, and omnivores using peer-reviewed literature (Supplementary Table 3). The polychaete feeding guild catalogue of Jumars et al. (2015) was used to classify the feeding types of polychaetes on family level. Isopods were grouped in the feeding types (selective, non-selective) deposit feeders based on the genera present in the GSR exploration license area (de Smet et al., 2017) and using information on feeding type and food sources presented in Menzies (1962).

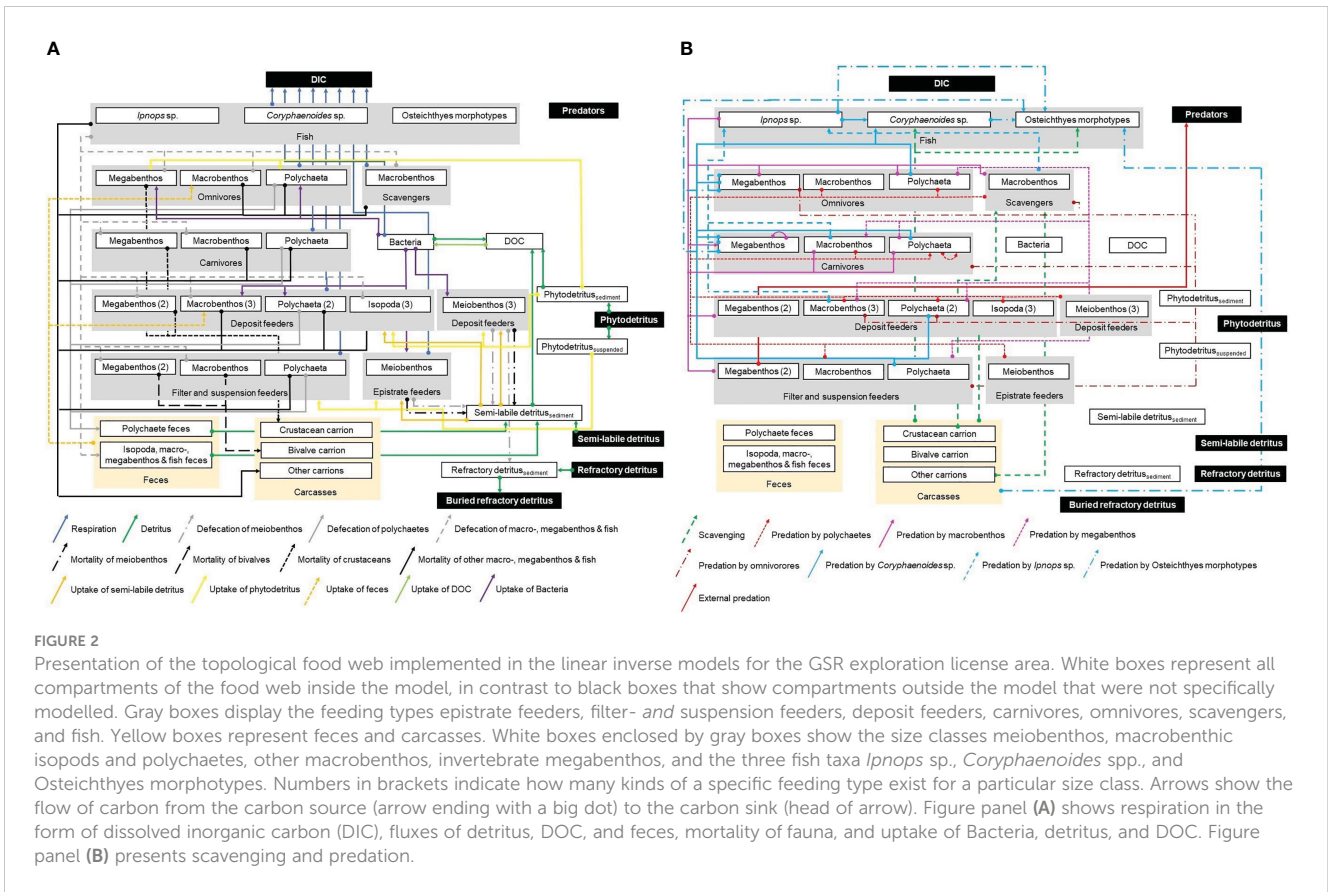
Invertebrate megabenthos ($>5 \text{ cm}$) comprised decapods, anthozoans and hydrozoans, poriferans, and echinoderms, i.e., crinoids, echinoids, holothurians, and ophiuroids (de Smet et al., 2021). These taxa were classified as deposit feeders, carnivorous suspension feeders, filter and suspension feeders, omnivores, and carnivores based on peer-reviewed literature (Supplementary Table 4). The fish observed in the GSR exploration area were *Coryphaenoides* spp., *Ipnopis* sp., and Osteichthyes morphotypes (de Smet et al., 2021) feeding on fish, crustaceans, polychaetes, and carrion (Supplementary Table 5). A detailed list with taxon-specific feeding types and prey as well as food sources, respectively, is presented in Supplementary Tables 2–5.

2.3 Food-web links

Links of carbon transfer between the food-web compartments were implemented as presented in Figure 2.

The sedimentary phytodetritus pool receives carbon input *via* degrading phytoplankton in marine snow, the semi-labile and refractory detritus pools are maintained by marine snow particles. Furthermore, fecal pellets, that are not taken up by specialized coprophagus feeders (i.e., organisms feeding on feces), contribute to the semi-labile and refractory detritus pool. Also dying metazoan meiobenthos becomes part of the semi-labile detritus pool. Dead macrobenthos, invertebrate megabenthos, and fish, in contrast, add to the carrion pool. All three detritus pools hydrolyze to DOC that is taken up by bacteria. Bacteria convert this DOC to dissolved inorganic carbon (DIC) *via* respiration and they contribute to the DOC pool when they burst due to virus-induced bacterial lysis. Carbon is lost from the modeled system *via* burial of refractory detritus, respiration of all fauna and bacteria, and by external predators that predate upon invertebrate megabenthos.

Deposit feeders graze upon bacteria, semi-labile detritus, and phytodetritus. Suspension and filter feeders filter, depending on the taxon, marine snow, crustaceans of macrobenthic size and fish out of the water column. Porifera, i.e., *Chonelasma* sp., *Docosaccus* sp., *Euplectella* sp., and other unidentified poriferans, furthermore, take up marine snow and DOC. Carnivores predate upon their specialized prey reported in Supplementary Tables 3, 4, except for the polychaetes of the family Sigalionidae, for which no prey types were published. Hence, this compartment was defined to feed on prey of the same size class. The diet composition of the individual fish taxa was constrained based on the contribution of each prey



taxon to the total prey carbon stock (Supplementary Table 5); the contribution of carrion to the fish diet, however, was not further constrained.

2.4 Data sources

2.4.1 Carbon stocks of food-web compartments

Data on carbon stocks of the various food-web compartments were extracted from the literature and standardized to mmol C m⁻² as described below.

The phytodetritus carbon stock in the upper 5 cm of sediment was calculated by converting the chlorophyll content [3.80 × 10⁻⁴ µg dry mass sediment⁻¹, (Pasotti et al., 2021)] measured by high performance liquid chromatography to carbon units using a carbon:chlorophyll a-ratio of 40 (de Jonge, 1980) and a porosity of 0.858 (B4S03) and of 0.874 (B6S02) (de Smet et al., 2017) assuming a dry sediment density of 2.55 g cm⁻³. Unfortunately, no chlorophyll a concentration data was available for B6S02, so that the concentration from B4S03 was also used for B6S02. No data on semi-labile detritus, here defined as the so-called biopolymeric carbon (Fabiano et al., 1995), i.e., the sum of proteins, carbohydrates, and lipids, existed for the GSR exploration license area or any other license area in the CCZ. Therefore, the sum of the semi-labile and refractory detritus carbon stock was calculated by subtracting the phytodetritus pool from the total organic carbon

(TOC) stock based on TOC data from de Smet et al. (2017). Subsequently, the relation of semi-labile to refractory detritus of 1:17.3 from the Peru Basin (SE Pacific) (de Jonge et al., 2020) was used to calculate both carbon stocks.

Bacterial carbon stock in the upper 5 cm of sediment was measured by Pape et al. (2017) as polar lipid concentrations following the Bligh and Dyer method (Bligh and Dyer, 1959; Boschker et al., 1999) and subsequently converted to bacterial biomass by the authors using conversion factors from Middelburg et al. (2000) and Brinch-Iversen and King (1990).

Metazoan meiobenthos carbon stock in the upper 5 cm of sediment was calculated by multiplying meiobenthos densities determined in multicorer samples (inner core diameter: 10 cm; n = 3) by Pape et al. (2017) with taxon-specific individual biomass data from Supplementary Table 2. Macrobenthos carbon stock in the upper 10 cm of sediment was estimated by multiplying macrobenthos density data taken from box corer deployments (surface: 0.25 m², sediment depth: 60 cm; n = 4 at B4S03, n = 3 at B6S02) by de Smet et al. (2017) with taxon-specific individual biomasses from Supplementary Table 3. Invertebrate megabenthos and fish density data were taken from an autonomous underwater vehicle megafauna survey of the seafloor in 6 m altitude (de Smet et al., 2021) and multiplied with taxon-specific individual biomasses from Supplementary Table 4 to estimate invertebrate megabenthos and fish carbon stocks. A complete list with carbon stocks of all food-web compartments is presented in Table 1.

TABLE 1 Carbon stocks (mmol C m⁻²) of all food-web compartments at sites B4S03 and B6S02 of the GSR exploration license area.

Compartment	B4S03	B6S02
Detritus		
Phytodetritus (PhytoDet)	2.29×10^{-2}	2.03×10^{-2}
Semi-labile detritus (slDet)	522	445
Refractory detritus (rDet)	8,412	7,170
Bacteria		
Bacteria (Bac)	34.7	19.8
Metazoan meiobenthos		
Deposit-feeding meiobenthos (MeiDF)	0.84	0.78
Epistrate-feeding Nematoda (NEMeDF; Phylum: Nematoda)	3.39×10^{-2}	8.18×10^{-2}
Non-selective deposit feeding Nematoda (NEMnsDF; Phylum: Nematoda)	0.13	0.26
Selective deposit feeding Nematoda (NEMsDF; Phylum: Nematoda)	2.88×10^{-2}	6.90×10^{-2}
Macrobenthos		
Oligochaeta (Mac_Oli; Phylum: Annelida, Class: Clitellata, Subclass: Oligochaeta)	1.81×10^{-3}	0.00
Copepoda (Mac_Cope; Phylum: Arthropoda, Class: Copepoda)	6.11×10^{-2}	5.28×10^{-2}
Amphipoda (Mac_Amp; Phylum: Arthropoda, Class: Amphipoda)*	3.43×10^{-2}	4.42×10^{-2}
Cumacea (Mac_Cum; Phylum: Arthropoda, Class: Malacostraca, Order: Cumacea)	0.00	3.09×10^{-3}
Mysida (Mac_Mys; Phylum: Arthropoda, Class: Malacostraca, Order: Mysida)	3.83×10^{-3}	5.74×10^{-3}
Tanaidacea (Mac_Tan; Phylum: Arthropoda, Class: Malacostraca, Order: Tanaidacea)	0.24	0.36
Ostracoda (Mac_Ost; Phylum: Arthropoda, Class: Ostracoda)	6.05×10^{-3}	2.72×10^{-2}
Pycnogonida (Mac_Pyc; Phylum: Arthropoda, Class: Pycnogonida)	3.83×10^{-3}	0.00
Other Crustacea (Mac_otherCru; Phylum: Arthropoda, Subphylum: Crustacea)	3.71×10^{-3}	8.34×10^{-3}
Bivalvia (Mac_Biv; Phylum: Mollusca, Class: Bivalvia)	1.50×10^{-2}	8.46×10^{-3}
Brachiopoda (Mac_Bra; Phylum: Brachiopoda)*	1.05×10^{-2}	7.87×10^{-3}
Nematoda (Mac_Nema; Phylum: Nematoda)	0.12	0.13
Nemertea (Mac_Neme; Phylum: Nemertea)	5.25×10^{-2}	7.87×10^{-3}
Ophiuroidea (Mac_Oph; Phylum: Echinodermata, Class: Ophiuroidea)	9.13×10^{-3}	2.74×10^{-3}
Scaphopoda (Mac_Sca; Phylum: Mollusca, Class: Scaphopoda)	2.59×10^{-2}	3.88×10^{-2}
Gastropoda (Mac_Gas; Phylum: Mollusca, Class: Mollusca)	0.46	0.09
Sipuncula (Mac_Sip; Phylum: Annelida, Order: Sipuncula)	1.05×10^{-2}	7.87×10^{-3}
Isopoda (Phylum: Arthropoda, Class: Malacostraca, Order: Isopoda)		
Deposit-feeding Isopoda (IsoDF)	0.80	1.11
Non-selective deposit feeding Isopoda (IsonDF)	0.11	8.56×10^{-2}
Selective deposit-feeding Isopoda (IseDF)	0.34	0.26
Polychaetes (Phylum: Annelida, Class: Polychaeta)		
Acroirridae (Pol_Acro)	1.77×10^{-2}	1.33×10^{-2}
Capitellidae (Pol_Cap)	1.77×10^{-2}	2.66×10^{-2}
Cirratulidae (Pol_Cir)	3.15×10^{-3}	6.70×10^{-3}
Euphrosinidae (Pol_Eup)	1.77×10^{-2}	1.33×10^{-2}
Glyceridae (Pol_Gly)	1.77×10^{-2}	0.00

(Continued)

TABLE 1 Continued

Compartment	B4S03	B6S02
Goniadidae (Pol_Goni)	2.22×10^{-2}	3.33×10^{-2}
Lumbrineridae (Pol_Lumb)	6.67×10^{-3}	5.0010^{-4}
Maldanidae (Pol_Mal)	0.15	0.00
Nephtyidae (Pol_Nep)	1.77×10^{-2}	0.00
Nereididae (Pol_Ner)	2.92×10^{-2}	7.30×10^{-3}
Opheliidae (Pol_Ophe)	2.66×10^{-2}	6.65×10^{-3}
Oweniidae (Pol_Owen)	1.53×10^{-3}	1.15×10^{-3}
Paraonidae (Pol_Para)	4.48×10^{-3}	5.04×10^{-3}
Phyllodocidae (Pol_Phy)	2.66×10^{-2}	6.65×10^{-3}
Sabellidae (Pol_Sab)	0.00	1.33×10^{-2}
Sigalionidae (Pol_Siga)	1.77×10^{-2}	0.00
Spionidae (Pol_Spio)	6.93×10^{-2}	0.12
Syllidae (Pol_Syl)	1.77×10^{-2}	0.00
Trichobranchidae (Pol_Tri)	1.06×10^{-2}	0.00
Invertebrate megabenthos		
Polychaeta (Meg_Pol; Phylum: Annelida, Order: Polychaeta)	8.07×10^{-3}	9.94×10^{-3}
Brisingida (Meg_Bri; Phylum: Echinodermata, Class: Asterozoa, Order: Brisingida)*	0.00	1.24
Other Asterozoa (Meg_othAs; Phylum: Echinodermata, Class: Asterozoa)	0.26	0.53
Crinozoa (Meg_Cri; Phylum: Echinodermata, Class: Crinozoa)*	7.14×10^{-3}	5.12×10^{-3}
Aspidodiadematidae (Meg_Asp; Phylum: Echinodermata, Class: Echinozoa, Order: Aspidodiadematoida, Family: Aspidodiadematidae)	0.16	5.50×10^{-2}
Ophiurozoa (Meg_Oph; Phylum: Echinodermata, Class: Ophiurozoa)	0.70	1.02
Bivalvia (Meg_Biv; Phylum: Mollusca, Class: Bivalvia)	1.25×10^{-2}	0.00
Other Mollusca (Meg_othMol; Phylum: Mollusca)	5.82×10^{-3}	0.00
Megabenthic crustaceans (Phylum: Arthropoda, Subphylum: Crustacea)		
Aristeidae (Meg_Ari)	0.23	3.73×10^{-2}
Galatheidae (Meg_Gal)	0.81	0.59
Other Decapoda (Meg_othDec)	5.62×10^{-3}	1.00×10^{-2}
Megabenthic cnidarians (Phylum: Cnidaria)		
Actiniaria (Meg_Act)*	6.34×10^{-3}	8.22×10^{-3}
Antipatharia (Meg_Ant)	0.28	0.42
Alcyonacea (Meg_Alc)	1.37×10^{-2}	9.41×10^{-2}
Ceriantharia (Meg_Cer)	0.00	0.92
Other Anthozoa (Meg_othAn)	6.80×10^{-2}	0.18
Hydrozoa (Meg_Hyd)	0.00	1.75×10^{-3}
Other Cnidaria (Meg_othCni)	6.24×10^{-5}	0.00
Holothurians (Phylum: Echinodermata, Class: Holothurozoa)		
Elpidiidae gen. sp. 2 (“double velum” morphotype in ccfzatlus.com) (Meg_Elp)	0.00	1.06×10^{-2}
Other Elpidiidae (Meg_othEl)	0.00	5.28×10^{-3}
Unknown Holothurozoa (Meg_unHo)	3.17×10^{-2}	1.80×10^{-2}

(Continued)

TABLE 1 Continued

Compartment	B4S03	B6S02
Poriferans (Phylum: Porifera)		
<i>Chonelasma</i> sp. (Meg_Cho)	1.01×10^{-2}	1.86×10^{-2}
<i>Docosaccus</i> sp. (Meg_Doc)	1.09×10^{-2}	1.63×10^{-2}
<i>Euplectella</i> sp. (Meg_Eup)	1.43×10^{-2}	3.24×10^{-3}
Other Porifera (Meg_othPor)	2.90×10^{-2}	3.24×10^{-2}
Fish		
<i>Coryphaenoides</i> spp. (Fish_Cor; Phylum: Chordata, Class: Teleostei, Order: Gadiformes, Family: Macrouridae, Genus: Coryphaenoides)	1.49	1.38
<i>Ipnops</i> sp. (Fish_Ipn; Phylum: Chordata, Class: Teleostei, Order: Aulopiformes, Family: Ipnopidae, Genus: Ipnops)	0.19	6.15×10^{-2}
Osteichthyes morphotypes (Fish_Ost; Phylum: Chordata, Parvphylum: Osteichthyes)	0.37	0.35

*Taxa excluded in the models developed for section 3.5.

2.4.2 Site-specific flux constraints

Site-specific flux constraints were estimated by Volz et al. (2018) in a numerical diagenetic model for the GSR exploration license area and were implemented in the food-web models as presented in Table 2.

Phytodetritus deposition corresponds to labile detritus deposition in Volz et al. (2018) and semi-labile and refractory detritus deposition rates are the influx of semi-labile and refractory marine snow particles. Phytodetritus and semi-labile detritus degradation processes describe the reduction of these detritus pools by dissolution of the detritus to DOC and their uptake by fauna. Refractory detritus is degraded via dissolution of this pool to DOC, and it is buried in the sediment via the burial flux. Total C mineralization relates to aerobic respiration that is responsible for 90% of the organic matter consumption at the seafloor in the CCZ (Volz et al., 2018).

2.4.3 Physiological constraints

Constraints of physiological processes that were included in the model are presented in Table 3.

Bacterial growth efficiency *BGE* is defined as

$$BGE = \frac{BCP}{(BCP + BR)} \quad (\text{Equation 1}),$$

with *BCP* being bacterial carbon production ($\text{mmol C m}^{-2} \text{d}^{-1}$) and *BR* being bacterial respiration ($\text{mmol C m}^{-2} \text{d}^{-1}$).

Assimilation efficiency *AE* is defined as

$$AE = \frac{(I - F)}{I} \quad (\text{Equation 2}),$$

where *I* is food ingested and *F* relates to the feces produced (Crisp, 1971).

Net growth efficiency *NGE* is defined as $NGE = \frac{G}{(G+R)}$ (Equation 3), where *G* is the growth and *R* is the respiration (Clausen and Riisgård, 1996).

The secondary production *SP* ($\text{mmol C m}^{-2} \text{d}^{-1}$) is calculated as

$$SP = \frac{P}{B} \text{ratio} \times C \text{ stock} \quad (\text{Equation 4}),$$

with $\frac{P}{B}$ ratio being the production/biomass ratio (d^{-1}).

The mortality *M* ($\text{mmol C m}^{-2} \text{d}^{-1}$) always ranges from 0 to the maximum secondary production. Respiration *R* is calculated similar to secondary production as:

$$R = r \times C \text{ stock} \quad (\text{Equation 5}),$$

where *r* corresponds to the biomass-specific faunal respiration (d^{-1}).

TABLE 2 Carbon flux data ($\text{mmol C m}^{-2} \text{d}^{-1}$) from Volz et al. (2018) were implemented in the model as equalities (single value) or inequalities [min, max]. .

Carbon flux	Value
Phytodetritus deposition	[0, 0.118]
Semi-labile detritus deposition	[0, 7.945×10^{-3}]
Refractory detritus deposition	[4.658×10^{-4} , ∞]*
Phytodetritus degradation	lDet stock \times [0, 5.479×10^{-5}]
Semi-labile detritus degradation	slDet stock \times [1.918×10^{-8} , ∞]*
Refractory detritus degradation	rDet stock \times [5.479×10^{-10} , ∞]*
Burial flux of refractory detritus	[0.013, ∞]*
Total C mineralization	[7.75×10^{-2} , 0.115]

*Constraints adjusted in the fitting step.

TABLE 3 Constraints of the physiological processes bacterial growth efficiency *BGE* (-), virus-induced bacterial mortality *VIBM* (-), bacteria carbon production *BCP* (mmol C m⁻² d⁻¹), assimilation efficiency *AE* (-), net growth efficiency *NGE* (-), secondary production *SP* (mmol C m⁻² d⁻¹), mortality *M* (mmol C m⁻² d⁻¹), respiration *R* (mmol C m⁻² d⁻¹), and feeding preferences *FP* (-) implemented in the food-web models as equalities (single values) and inequalities ([minimum, maximum] values).

Physiological process	Size class	Value	Ref.
<i>BGE</i>	Bacteria	[0.27, 0.90]*	1,2
<i>VIBM</i>	Bacteria	[0.87, 0.91]	3
<i>BCP</i>	Bacteria	[0.34, 0.68]	1,3
<i>AE</i>	Metazoan meiobenthos	[0.18, 0.27]	2
	Macrobenthos	[0.68, 0.89]	2
	Invertebrate megabenthos	[0.40, 0.75]	2
	Fish	[0.84, 0.87]	2
<i>NGE</i>	Metazoan meiobenthos	[0.10, 0.96]	2
	Macrobenthos	[0.57, 0.68]	2
	Invertebrate megabenthos	[0.23, 0.61]	2
	Fish	[0.37, 0.71]	2
<i>SP</i>	Metazoan meiobenthos	[2.00 × 10 ⁻² , 0.12] × C stock	2
	Macrobenthos	[2.57 × 10 ⁻³ , 1.67 × 10 ⁻²] × C stock	2
	Invertebrate megabenthos	[3.18 × 10 ⁻⁴ , 1.47 × 10 ⁻³] × C stock	2
	Fish	[0, 6.30 × 10 ⁻⁴] × C stock	2
<i>M</i>	Metazoan meiobenthos	[0, 0.12] × C stock	2
	Macrobenthos	[0, 1.67 × 10 ⁻²] × C stock	2
	Invertebrate megabenthos	[0, 1.47 × 10 ⁻³] × C stock	2
	Fish	[0, 6.30 × 10 ⁻⁴] × C stock	2
<i>R</i>	Metazoan meiobenthos	[7.00 × 10 ⁻³ , 0.15] × C stock	2
	Macrobenthos	[3.57 × 10 ⁻⁵ , 4.21 × 10 ⁻²] × C stock	2
	Invertebrate megabenthos	[9.32 × 10 ⁻⁸ , 1.26 × 10 ⁻³] × C stock	2
	<i>Coryphaenoides</i> spp., Osteichthyes morphotypes	[3.12 × 10 ⁻⁴ , 4.84 × 10 ⁻⁴] × C stock	4-7
	<i>Ipnops</i> sp.	[1.79 × 10 ⁻⁴ , 8.54 × 10 ⁻⁴] × C stock	2
<i>FP</i>		[0.75, 1.00]	2

*Constraint adjusted in the fitting step.

In several cases, individual faunal constraints had to be adjusted in the fitting step. For these cases, the adjusted constraints are presented in Supplementary Table 6.

References (Ref.): ¹(Vonnahme et al., 2020), ²(de Jonge et al., 2020), ³(Danovaro et al., 2008), ⁴(Smith, 1978), ⁵(Drazen and Seibel, 2007), ⁶(Smith and Hessler, 1974), ⁷(Drazen and Yeh, 2012).

Feeding preferences *FP* of mixed deposit feeders and carnivores and omnivores indicate the contribution of predation to their respective diets.

$$E \times x = f \quad (\text{Equation 6}),$$

$$G \times x \geq h \quad (\text{Equation 7}),$$

2.5 Linear inverse model development and network indices

Carbon-based linear inverse food-web models were developed for steady state conditions based on the topological food web presented in Figure 2. These food-web models consist of linear functions in the form of equality (equation 6) and inequality matrix equations (equation 7) (van Oevelen et al., 2010):

with vector x including the unknown fluxes. The vectors f and h include empirical equality and inequality data, and the coefficients in the matrices E and G describe combinations of unknown fluxes that have to fulfill the requirements defined in the vectors f and h .

Models for the two sites consisted of 654 (B6S02)–829 (B4S03) flows, 74 (B6S02)–79 (B4S03) mass balances (i.e., food-web compartments), 0 data equalities, and 340 (B6S02)–371 (B4S03) data inequalities. This meant that the models were mathematically under-determined (74–79 equalities vs. 654–829 unknown flows). In

this case, either a single ‘best’ solution can be calculated based on the principle of parsimony or simplicity, or the uncertainty of each flow can be quantified using the likelihood approach (van Oevelen et al., 2010). Generally, the likelihood approach is recommended (van Oevelen et al., 2010), but this can be extremely computational demanding when the food-web models are exceptionally complex (see e.g. de Smet et al. (2016)). In fact, a test run on the bioinformatics server of the NIOZ Royal Netherlands Institute for Sea Research (The Netherlands) with 2,000 solutions calculated in one session required more than 1.5 months of calculation. As a result, the author decided to calculate the parsimonious solution of each food-web model and estimate ranges with the R package *LIM* v.1.4.6 (van Oevelen et al., 2010) in R v.1.3.1073 (R-Core Team, 2017). These ranges are reported for each flux in the supplementary material.

The network indices “number of links” L_{total} , “link density” LD , “connectance” C , “total system throughput” T , which is the sum of all carbon flows in the food web, Finn’s Cycling Index FCI , and the trophic level of each compartment were calculated using the R package *NetIndices* v.1.4.4 (Kones et al., 2009).

The trophic levels of the carrion pools were calculated as described in de Jonge et al. (2020) as:

$$TL_{carrion} = \sum_{j=1}^n \left(\frac{T_{j, carrion}^*}{T_{carrion}} \times TL_j \right) \quad , \quad (\text{Equation 8}),$$

where n corresponds to the number of internal food-web compartments, j is all food-web compartments, T^* is the flow matrix without external flows, and $T_{carrion}$ is the total carbon inflow to the carrion pool without external sources.

3 Results

3.1 Benthic biomass

Total carbon stocks were 8,977 mmol C m⁻² at site B4S03 and 7,646 mmol C m⁻² at B6S02 (Table 1). Most of these carbon stocks consisted of semi-labile (B4S03: 5.81%, B6S02: 5.82%) and refractory detritus (B4S03: 93.7%, B6S02: 93.8%). Phytodetritus, bacteria, and metazoan fauna accounted for, respectively, 2.55 × 10⁻⁴% (B4S03)–2.66 × 10⁻⁴% (B6S02), 0.26% (B6S02)–0.39% (B4S03), and 0.10% (B4S03)–0.14% (B6S02) of the total carbon stock.

Nematoda accounted for 0.19 mmol C m⁻² and 0.41 mmol C m⁻² of the carbon stocks at B4S03 and B6S02, respectively, while other meiobenthos (i.e., copepods and their nauplii) accounted for 0.84 mmol C m⁻² and 0.78 mmol C m⁻² (Figure 3). The carbon stock of macrobenthic Isopoda was 1.25 mmol C m⁻² and 1.46 mmol C m⁻² at the two different sites and macrobenthic polychaetes had a carbon stock of 0.47 mmol C m⁻² and 0.25 mmol C m⁻² at B4S03 and B6S02, respectively (Figure 3). The other macrobenthos carbon stock included mainly macrobenthic Nematoda, Tanaidacea, and Gastropoda, that contributed between 23.2% (B6S02) and 29.5% (B4S03) to the total carbon stock of this size class. The megabenthic carbon stock accounted for 2.71 mmol C m⁻² at the B4S03 site and 5.23 mmol C m⁻² at the B6S02 site (Figure 3). Fish had a carbon stock of 2.05 mmol C m⁻² and 1.79 mmol C m⁻² (Figure 3).

3.2 Food-web structure and trophic levels

The food webs consisted of 75 and 71 compartments at sites B4S03 and B6S02 that were connected with 336 and 303 links, respectively (Figure 4; Table 4), resulting in a link density of 4.48 at B4S03 and of 4.27 at B6S02. The connectance was 4.77 × 10⁻² at B4S03 and 4.75 × 10⁻² at B6S02.

Maximum trophic level was estimated as 4.22 (macrobenthic Ostracoda) at site B4S03 and as 4.61 (fish of the Osteichthyes morphotypes) at B6S02. Mean modelled trophic level of metazoan fauna ranged from 2.73 ± 0.08 (± standard error; B4S03) to 2.87 ± 0.10 (B6S02). Mean modelled trophic levels of exclusively carnivores were estimated to be 3.36 ± 0.08 and 3.55 ± 0.13 at site B4S03 and B6S02, respectively, and the modelled trophic levels of exclusively deposit feeders were estimated as 2.51 ± 7.75 × 10⁻² and 2.50 ± 8.56 × 10⁻².

3.3 Carbon flows

Modeled total carbon input, i.e., the deposition of detritus and filter- and suspension feeding, had an estimated value of 9.21 × 10⁻² mmol C m⁻² d⁻¹ at site B4S03 and of 9.15 × 10⁻² mmol C m⁻² d⁻¹ at B6S02 (Table 5). This input was dominated by phytodetritus deposition with a contribution of 58.3% (B6S02) to 61.8% (B4S03) to total deposition, followed by refractory detritus deposition (B4S03: 29.6%, B6S02: 33.0%). Additionally, an external pool of swimming copepods as prey for several predators (i.e., fish, antipatharians, hydrozoans, and other anthozoans) contributed 4.78 × 10⁻⁵ mmol C m⁻² d⁻¹ (B6S02) to 5.99 × 10⁻³ mmol C m⁻² d⁻¹ (B4S03) to the modelled benthic ecosystem.

Most carbon was estimated to be lost from the two sampling sites *via* respiration (85.8–86.7% of total carbon loss), whereas carbon burial accounted for 1.30 × 10⁻² mmol C m⁻² d⁻¹.

Estimated respiration ranged from 7.85 × 10⁻² mmol C m⁻² d⁻¹ (B6S02) to 8.51 × 10⁻² mmol C m⁻² d⁻¹ (B4S03). It was dominated by bacterial respiration that contributed between 44.1% (B4S03) and 48.1% (B6S02) to total respiration. Faunal respiration was estimated to be lower at B6S02 (4.08 × 10⁻² mmol C m⁻² d⁻¹) than at B4S03 (4.73 × 10⁻² mmol C m⁻² d⁻¹) and was dominated by metazoan meiobenthos at B6S02 and by metazoan meiobenthos and macrobenthos at B4S03 (Table 5).

Modeled carbon ingestion of fauna is summarized in Supplementary Figures 1–4. Estimated uptake of carbon by metazoan meiobenthos (Supplementary Figure 1) was largest and accounted for 8.63 × 10⁻² mmol C m⁻² d⁻¹ (B4S03) and 8.96 × 10⁻² mmol C m⁻² d⁻¹ (B6S02). Modeled carbon uptake by macrobenthos (Supplementary Figure 2; B4S03: 5.63 × 10⁻² mmol C m⁻² d⁻¹, B6S02: 3.84 × 10⁻² mmol C m⁻² d⁻¹) and megabenthos (Supplementary Figure 3; B4S03: 1.07 × 10⁻² mmol C m⁻² d⁻¹, B6S02: 3.51 × 10⁻² mmol C m⁻² d⁻¹) were of similar magnitude. The estimated carbon uptake of fish (Supplementary Figure 4) was, however, one order of magnitude lower (B4S03: 2.54 × 10⁻³ mmol C m⁻² d⁻¹, B6S02: 1.54 × 10⁻³ mmol C m⁻² d⁻¹).

Macrobenthic polychaetes were responsible for 6.37–11.8%, macrobenthic isotopes for 7.81–8.56%, and other macrobenthos

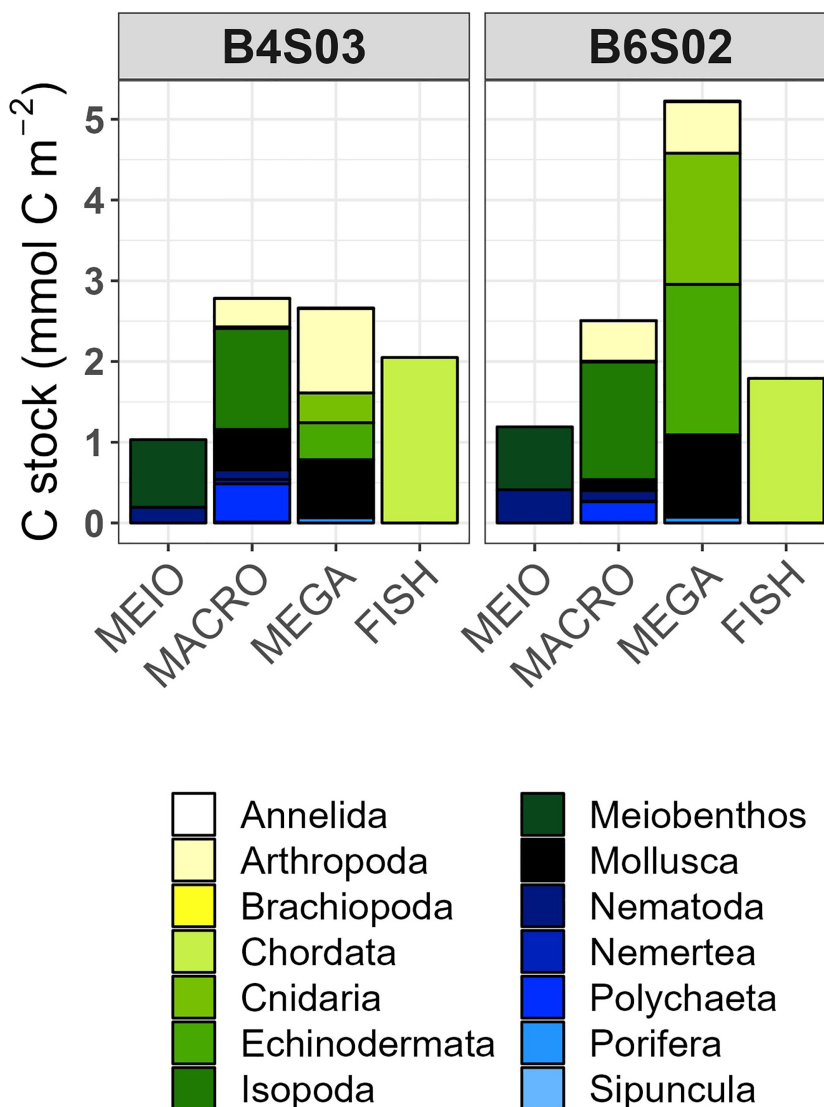


FIGURE 3
 Mean carbon stocks (mmol C m⁻²) of the faunal food-web compartments at sites B4S03 (left columns) and B6S02 (right columns) in the GSR exploration license area.

for 9.13–15.7% of carbon uptake. Megabenthic crustaceans were responsible for 1.40–2.02%, megabenthic cnidarians for 3.29–4.71%, holothurians for 7.40×10^{-2} –8.62%, poriferans for 0.28–1.17%, and all other invertebrate megabenthos for 1.21–5.45% of total faunal ingestion.

Uptake of DOC by bacteria as part of the microbial loop (see section 3.4) was 0.38 mmol C m⁻² d⁻¹.

3.4 Carbon cycling and specific C pathways

T. was estimated to be 1.18 mmol C m⁻² d⁻¹ at site B4S03 and 1.20 mmol C m⁻² d⁻¹ at B6S02 and *FCI* was modeled to range from 0.53 mmol C m⁻² d⁻¹ (B4S03) to 0.53 mmol C m⁻² d⁻¹ (B6S02).

The microbial loop, i.e., dissolution of detritus, uptake of DOC by bacteria, virus-induced bacterial mortality, bacterial respiration,

and faunal grazing upon bacteria, had an estimated carbon flow of 0.84 mmol C m⁻² d⁻¹, which was 71.2% of modelled *T.* at B4S03 and 69.8% of modelled *T.* at B6S02.

An estimated carbon flow of 2.55×10^{-3} mmol C m⁻² d⁻¹ was channeled through the scavenging loop (i.e. scavenging of scavengers on carrion) at B4S03, which was 0.22% of modelled *T.* At B6S02, the carbon flow through the scavenging loop was modeled to be 7.25×10^{-4} mmol C m⁻² d⁻¹ (6.19×10^{-2} % of modelled *T.*).

3.5 Consequences of polymetallic nodule removal

Excluding fauna from the food webs that have been predicted to be lost when polymetallic nodules are removed (Stratmann et al., 2021), led to a decrease in number of food-web compartments of 5.33% (B4S03) to 7.04% (B6S02) and to a loss of 5.28% (B6S02) to

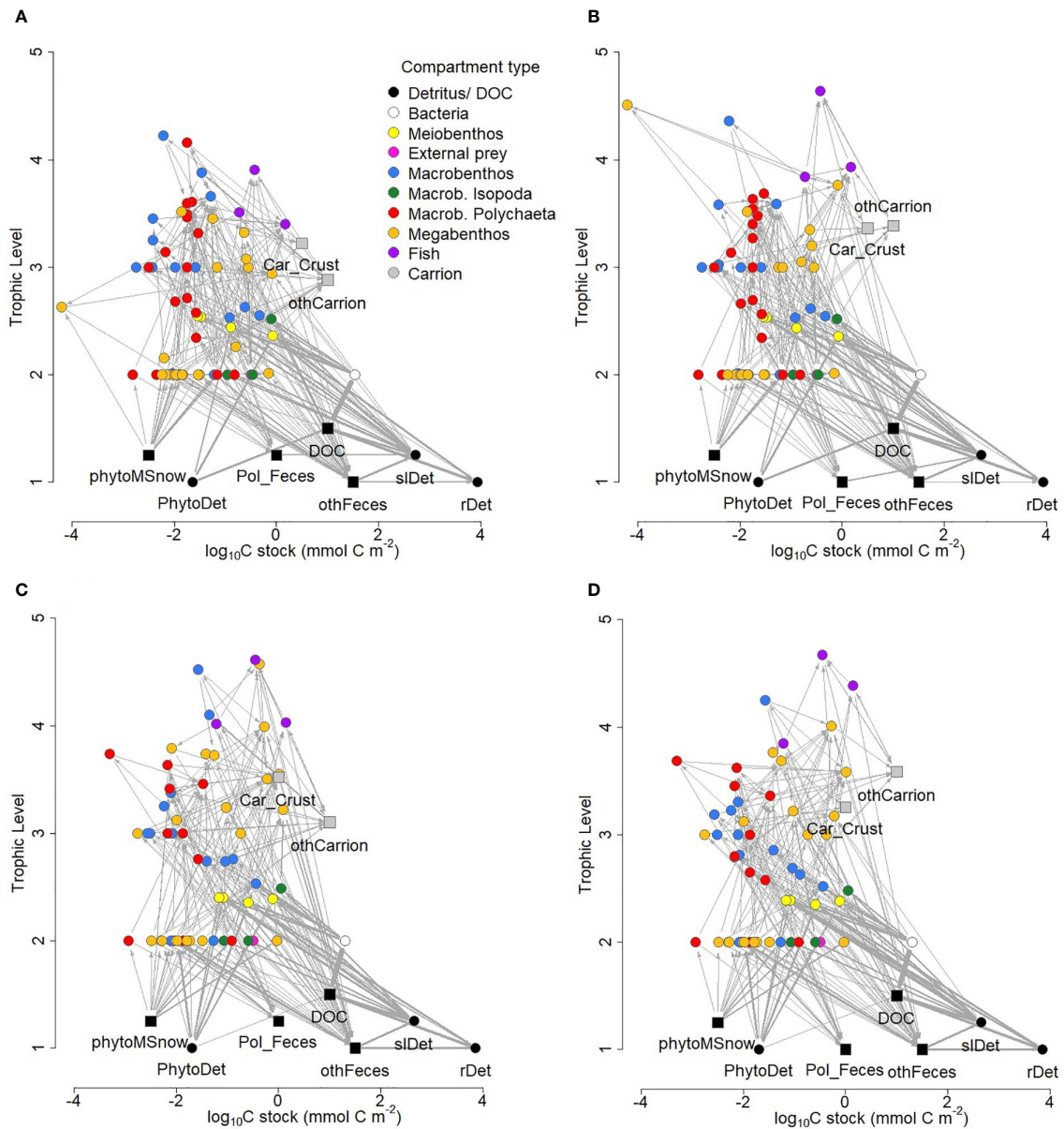


FIGURE 4

Structure of food-web models developed for the B4S03 site (A) in the presence and (B) absence of polymetallic nodules and for the B6S02 site (C) in the presence and (D) absence of nodules in the GSR exploration license area. Round nodes show compartments whose biomass (mmol C) is known, whereas square nodes indicate compartments to which the author assigned values for plotting purposes. Trophic levels 1.25 and 1.5 were assigned to square nodes for plotting purposes only; their true trophic levels are 1. The thickness of the arrows corresponds to the magnitude of carbon flow ($\text{mmol C m}^{-2} \text{d}^{-1}$) between two food-web compartments after double square root-transformation. Note, that neither import nor export fluxes were plotted and that the x-axis is a \log_{10} scale. Car_Crust = crustacean carrion, DOC = dissolved organic carbon, othCarrion = other carrion, othFeces = isopod, macro-, invertebrate megabenthic and fish feces, PhytoDet = phytodetritus, phytoMSnow = phytodetritus-based marine snow, Pol_Feces = polychaete feces, rDet = refractory detritus, siDet = semi-labile detritus.

9.23% (B4S03) of all links. Link density was reduced by 4.11% at B4S03 and increased by 1.90% at B6S02, and the connectance increased by 0.29% (B4S03) to 10.5% (B6S02). T_i decreased by 0.27% at B4S03 and increased by $2.52 \times 10^{-2}\%$ at B6S02, and FCI increased by 0.29% (B6S02) to 0.34% (B4S03). Network indices calculated for both sites in the presence and absence of nodule-related fauna are reported in Table 4.

A summary of the most important changes in modelled carbon flows (ΔC_{flow}) due to the exclusion of nodule-dependent fauna is

visualized in Figure 5. At site B4S03, the largest changes in carbon flows were related to increased respiration of macrobenthic polychaetes ($+3.64 \times 10^{-3} \text{ mmol C m}^{-2} \text{d}^{-1}$) and decreased predation of fish upon macrobenthic polychaetes ($-3.63 \times 10^{-3} \text{ mmol C m}^{-2} \text{d}^{-1}$). In comparison, at B6S02, the largest change in carbon flows was related to the increased sedimentary detritus uptake by metazoan meiobenthos ($+6.13 \times 10^{-3} \text{ mmol C m}^{-2} \text{d}^{-1}$) and increased predation of megabenthic cnidarians on macrobenthic isopods ($+3.90 \times 10^{-3} \text{ mmol C m}^{-2} \text{d}^{-1}$).

TABLE 4 Network indices calculated for the sites B4S03 and B6S02 when all fauna are present (+nodule) and when fauna predicted to be lost when polymetallic nodules are removed are excluded (-nodule). Relative changes (%) in network indices due to faunal loss are reported for each site.

Network indices	B4S03 site			B6S02 site		
	(+nodule)	(-nodule)	% relative change	(+nodule)	(-nodule)	% relative change
<i>n</i>	75	71	-5.33	71	66	-7.04
<i>L_{total}</i>	336	305	-9.23	303	287	-5.28
<i>LD</i>	4.48	4.30	-4.11	4.27	4.35	+1.90
<i>C</i>	4.77×10^{-2}	4.79×10^{-2}	+0.29	4.75×10^{-2}	5.24×10^{-2}	+10.5
<i>T.</i>	1.18	1.17	-0.27	1.20	1.20	$+2.52 \times 10^{-2}$
<i>FCI</i>	0.53	0.54	+0.34	0.53	0.53	+0.29

n = number of food-web compartments, *L_{total}* = number of links, *LD* = link density, *C* = connectance, *T.* = total system throughput, *FCI* = Finn's Cycling Index.

Removing the nodule-dependent fauna did not affect the strength of the microbial loop. In contrast, the scavenging loop at B4S03 (-nodule) (7.25×10^{-4} mmol C m⁻² d⁻¹) was only 28.4% of the original scavenging loop and at B6S02 (-nodule), the scavenging loop accounted for 43.5% ($= 1.51 \times 10^{-3}$ mmol C m⁻² d⁻¹) of the initial scavenging loop.

4 Discussion

The role played by nodule-dependent fauna in benthic carbon cycling in the eastern CCZ was assessed by investigating differences in modelled carbon flows of intact food webs and of food webs where

nodule-dependent fauna was excluded in the models. The food webs for two sites in the GSR exploration license area contained between 9 mmol C m⁻² and 11 mmol C m⁻² faunal carbon and between 20 mmol C m⁻² and 35 mmol C m⁻² bacterial carbon in 61 to 65 biotic compartments (excluding detritus, DOC, and carrion) (Figures 3, 4; Table 1). The food webs were estimated to be fueled to 58% to 62% by phytodetritus deposition and to 30% to 33% by refractory detritus deposition, whereas most of the carbon was lost from the food webs as respiration. This respiration was dominated by bacterial respiration, followed by metazoan meiobenthos, and other macrobenthos respiration. Removing nodule-dependent faunal compartments had almost no effect on total system throughput *T.*, but reduced the total number of links by 5% to 9% (Table 4).

TABLE 5 Deposition of detritus (phytodetritus, semi-labile detritus, refractory detritus) and respiration of bacteria, metazoan meiobenthos, fish, and different macro- and megabenthos faunal groups at sites B4S03 and B6S02.

	B4S03	%	B6S02	%
<i>Total deposition</i>	9.21×10^{-2}	100	9.15×10^{-2}	100
Phytodetritus	5.69×10^{-2}	61.8	5.33×10^{-2}	58.3
Semi-labile detritus	7.95×10^{-3}	8.63	7.94×10^{-3}	8.68
Refractory detritus	2.73×10^{-2}	29.6	3.02×10^{-2}	33.0
<i>Total respiration</i>	8.51×10^{-2}	100	7.85×10^{-2}	100
Bacteria	3.78×10^{-2}	44.4	3.78×10^{-2}	48.1
Metazoan meiobenthos	1.11×10^{-2}	13.0	2.00×10^{-2}	25.5
Macrobenthic polychaetes	1.09×10^{-2}	12.8	3.06×10^{-3}	3.90
Macrobenthic isopods	8.66×10^{-3}	10.2	4.92×10^{-3}	6.26
Macrobenthos (except polychaetes, isopods)	1.19×10^{-2}	14.0	5.25×10^{-3}	6.68
Megabenthic crustaceans	1.38×10^{-3}	1.62	8.03×10^{-4}	1.02
Megabenthic cnidarians	1.51×10^{-3}	1.78	2.05×10^{-3}	2.61
Holothurians	3.99×10^{-5}	4.69×10^{-2}	4.27×10^{-5}	5.44×10^{-2}
Poriferans	8.10×10^{-5}	9.52×10^{-2}	8.89×10^{-5}	0.11
Invertebrate megabenthos (except crustaceans, cnidarians, holothurians, poriferans)	9.51×10^{-4}	1.12	3.60×10^{-3}	4.59
Fish	8.58×10^{-4}	1.01	9.18×10^{-4}	1.17

Data are presented as flux values (mmol C m⁻² d⁻¹) and as % contribution to total deposition and total benthic respiration.

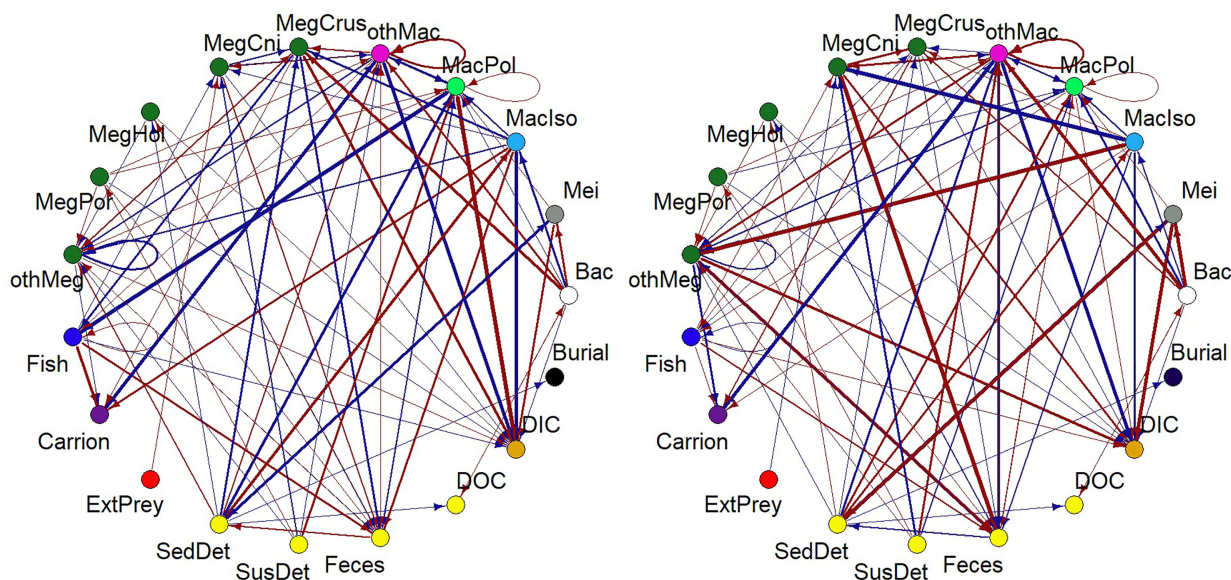


FIGURE 5

Figure summarizing changes in carbon flows between compartments because of the exclusion of polymetallic nodule-dependent fauna at sites (A) B4S03 and (B) B6S02. The width of the arrow corresponds to the double-square root of ΔC_{flow} (in $\text{mmol C m}^{-2} \text{d}^{-1}$), where $\Delta C_{\text{flow}} = C_{\text{flow}+\text{nodule}} - C_{\text{flow}-\text{nodule}}$, and the color indicates whether an exclusion of the fauna led to an increase in a specific carbon flow (red) or a decrease (blue). Bac, bacteria; ExtPrey, external prey; Maclso, macrobenthic isopods; MacPol, macrobenthic polychaetes; MegCni, megabenthic cnidarians; MegCrus, megabenthic crustaceans; MegHol, holothurians; MegPor, poriferans; Mei, metazoan meiobenthos; othMac, other macrobenthos; othMeg, invertebrate megabenthos; SedDet, sedimentary detritus; SusDet, suspended detritus.

4.1 Model limitations

Like all scientific models, these highly resolved food-web models have limitations.

Biomasses of metazoan meiobenthos, macrobenthos, invertebrate megabenthos, and fish were estimated by converting densities reported by the authors of the original peer-reviewed studies (see section 2.4.1) to carbon stocks using conversion factors (Supplementary Tables 2–4). de Smet et al. (2021) assessed invertebrate megabenthos community composition and densities using autonomous underwater vehicle imagery obtained from ~6 m above the seafloor and only reported specimens >5 cm. In a method paper, Schoening et al. (2020) compared abyssal faunal densities on seafloor images taken at 1.6 to 1.7 m above the seafloor with images taken 4.5 and 7.5 m above the seafloor and found three to 28 times higher densities in the low altitude images compared to the high-altitude images. Consequently, in this study invertebrate megabenthos biomasses and subsequently their role in carbon cycling are underestimated.

Polymetallic nodules in abyssal plains have microbial communities inside their crevices (Blöthe et al., 2015; Cho et al., 2018) and on their surfaces (Wang et al., 2009) that are different from the microbial community in adjacent sediments (Cho et al., 2018; Molari et al., 2020). Hence, for a proper assessment of the role of polymetallic nodules on abyssal carbon cycling, not only the impact of nodule-dependent fauna exclusion, but also the effect of nodule-dependent microorganism exclusion on carbon cycling should be assessed. However, so far, no study has quantified the role of these microorganisms in carbon cycling and data on

bacterial biomass inside and outside the nodules are lacking for the GSR exploration license area or any other license area in the CCZ. Therefore, I could not confidently include this process in the food web models for the sites B4S03 and B6S02, and used one (sedimentary) bacterial carbon pool per site instead.

Sweetman et al. (2019) measured $0.10 \pm 0.03 \text{ mmol C m}^{-2} \text{d}^{-1}$ DIC uptake by benthic bacteria in the UK Seabed Resources Ltd (UK1) exploration license area and the Ocean Minerals of Singapore exploration area in the eastern CCZ. This value was 1.2 to 2.0 times higher than the uptake of phytodetritus carbon by bacteria at the sites (Sweetman et al., 2019) and therefore likely a very substantial contribution to abyssal carbon cycling. However, as the researchers conducting the baseline studies for GSR at B4S03 and B6S02 did not investigate bacterial dissolved inorganic carbon uptake, I am hesitant to include this process in the model (see also discussion in de Jonge et al. (2020)). Further studies in dark carbon fixation at different sites of the CCZ would therefore provide valuable information about the underlying mechanisms and which microorganisms are involved in them and allow to include this process in future abyssal carbon-based food-web models.

Foraminiferans are one of the dominant compartments of meiobenthos (Gooday and Goineau, 2019), macrobenthos (Goineau and Gooday, 2017; Stachowska-Kamińska et al., 2022; Gooday and Wawrzyniak-Wydrowska, 2023), invertebrate megabenthos (Gooday et al., 2017; Simon-Lledó et al., 2019a; Simon-Lledó et al., 2019b), and nodule-encrusting communities (Veillette et al., 2007; Gooday et al., 2015) in the CCZ (Gooday et al., 2021). Nevertheless, their role in carbon cycling as well as the potential importance of small naked protists (i.e., ciliates, flagellates,

amoebae) for the microbial communities are almost always overlooked, except by a few specialists (Gooday et al., 2020; Gooday et al., 2021). Foraminiferans are particularly difficult to include in carbon-based food-web models as it is often difficult to determine the proportion of living vs. dead specimens. This applies to the large megabenthic xenophyophores visible in seafloor images (Hughes and Gooday, 2004) as well as to the smaller species. We also miss information about assimilation and net growth efficiencies, growth rates/secondary production, and mortality rates required to model them. Having said that, de Jonge et al. (2020) tried to estimate the contribution of foraminiferans to carbon cycling in the Peru Basin. These authors estimated that Xenophyophores take up $0.63 \text{ mmol C m}^{-2} \text{ d}^{-1}$ assuming that all Xenophyophores observed on still images were alive. Even though $T.$ in the Peru Basin is substantially larger than in the CCZ ($6.42 \text{ mmol C m}^{-2} \text{ d}^{-1}$ when dark carbon fixation and Xenophyophores were included, (de Jonge et al., 2020)), I expect a large underestimation of $T.$ for the sites B4S03 and B6S02 of up to 10% due to the neglect of foraminiferans.

4.2 Regional differences in carbon cycling at abyssal plains

The presented food webs estimated a difference in total system throughput $T.$ of $2.49 \times 10^{-2} \text{ mmol C m}^{-2} \text{ d}^{-1}$ between sites B4S03 and B6S02 (Table 4). This difference in $T.$ was partly the result of higher carbon cycling by deposit-feeding nematodes at B4S03 compared to B6S02 (Table 1) and might be related to small-scale variability in environmental parameters between the two sites. Metazoan meiobenthos densities in surface sediments (0–5 cm sediment depth) of the CCZ are influenced by water depth, silt content, and polymetallic nodule density (Hauquier et al., 2019). In a comparison of metazoan meiobenthos across various locations in the eastern CCZ, Hauquier et al. (2019) measured the highest meiobenthos density at a location with low nodule density, high pigment concentrations as a proxy for (fresh) phytodetritus availability, and low clay content compared to the other sampling locations. Further sediment characteristics that influence meiobenthos distribution and densities in the eastern CCZ were identified in a modeling exercise by Uhlenkott et al. (2021). They include total organic and inorganic carbon content of the sediment, dry bulk sediment density, and shear strength. In this study, site B4S03, where higher metazoan biomass was detected, was indeed characterized by decreased nodule abundance compared to the B6S02 site, though mud content was higher and total organic carbon content was lower at B4S03 than at B6S02 (de Smet et al., 2017).

Another reason for the differences in $T.$ was the higher carbon uptake by invertebrate megabenthos (i.e., cnidarians, holothurians, poriferans, other invertebrate megabenthos except crustaceans) at B6S02 compared to B4S03. Differences in invertebrate megabenthos and fish densities at various spatial scales have been described for the mid-eastern CCZ by (Simon-Lledó et al., 2020). The authors found that geomorphology and polymetallic nodule cover control faunal abundance and community composition, areas with the lowest nodule cover having consistently decreased faunal densities compared to areas

with higher nodule cover. Simon-Lledó et al. (2020) further speculated that the shape and volume of nodules might be important for community structure. The two study sites in the GSR exploration license area investigated in this study are also characterized by different nodule densities, volumes, and coverages, whereby nodule density is higher at B6S02, but nodule volume and coverage are lower. Hence, I conclude that environmental conditions and particularly polymetallic nodule densities exert an important influence on carbon cycling at a regional scale (280 km) in the eastern CCZ.

4.3 Assessment of polymetallic nodule removal on C cycling and outlook to prospective deep-seabed mining effects

Excluding nodule-dependent fauna from the food webs developed for sites B4S03 and B6S02 impacted the faunal contribution to $T.$, but had no effect on the microbial loop. The taxa, that were removed, belonged to filter and suspension feeders taking up marine snow (Brachiopoda, Crinoidea), but also to scavengers (Amphipoda observed always in pairs at sponge stalks; (Stratmann et al., 2021; personal observations)), and carnivorous suspension feeders (Brisingida, Actinaria) predated upon small crustaceans (Table 1, Supplementary Tables 3, 4).

Scavenging amphipods were responsible for 89% of scavenging occurring at B4S03, so that their absence as a result of nodule removal strongly reduced the scavenging loop. Scavengers in the CCZ include demersal fish, such as *Coryphaenoides* spp., *Bassozetus* sp., and *Pachycara nazca*, and invertebrate megabenthos, like the amphipod *Eurythenes gryllus*, squat lobster *Munidopsis* sp., and the shrimp *Cerataspis monstrosus* (Harbour et al., 2020). Their taxon density and diversity vary regionally and Drazen et al. (2021) observed that the scavenger assemblage in the eastern CCZ was very different from the assemblage in the western APEIs due to higher abundances of the shrimp *Hymenopenaeus nereus* and lower abundances of the fishes *Barathrites iris* and *Coryphaenoides* spp. The latter fish was also observed in the GSR exploration license area (de Smet et al., 2021) and the carbon-based food-web model for B4S03 estimated that *Coryphaenoides* spp. partly compensated the loss of scavenging amphipods by increasing its contribution to the scavenging loop from 0% to 44%.

Abyssal scavengers react relatively fast to the deposition of carrion at the seafloor: *Coryphaenoides* spp. were attracted to fish bait (i.e., albacore tuna) at the seafloor of the eastern CCZ within 1 h (Harbour et al., 2020) and synphobranchid eels reached the fish bait (i.e., Pacific mackerel) in the western CCZ after ~7 h (Leitner et al., 2020; Leitner et al., 2021). Also, during a natural mass deposition event of gelatinous pyrosome carcasses in the Peru Basin in 2015, actinarians, ophiuroids, asteroids, and isopods were observed to (putatively) scavenge on the pyrosomes carcasses within a couple of days (personal observation, Hoving et al. (in review)). Hence, an industrial deep-seabed mining operation will likely attract scavenging fish and invertebrate megabenthos within hours. For the first months to years, this will overcompensate the loss of nodule-dependent scavengers and the importance of the scavenging loop for benthic carbon cycling will strongly increase, unless scavengers are chased off

by the sediment plume or by the toxic metals that might be released during the mining operation (Koschinsky et al., 2001; Hauton et al., 2017; Müller et al., 2018).

At B4S03, filter and suspension feeding Bivalvia benefitted from the loss of nodule-dependent filter and suspension feeding Brachiopoda and Crinoidea by ingesting 8% more labile marine snow. More labile marine snow particles, that nodule-dependent filter and suspension feeders normally would have filtered out of the water column, however, settled on the sediment at B4S03 and at B6S02 where they contributed to the sedimentary phytodetritus pool. As a result, epistrate feeding, selective and non-selective deposit-feeding nematodes were estimated to consume more labile phytodetritus at B6S02, while deposit-feeding isopods, polychaetes of the family Maldanidae and non-selective deposit-feeding nematodes were predicted to feed on more labile phytodetritus at B4S03.

The top 1 m of seafloor sediment is assumed to contain 10^8 prokaryotic cells cm^{-3} (Jørgensen and Boetius, 2007) and Nomaki et al. (2021) measured prokaryotic cell abundances of 3.6×10^7 cells g^{-1} in the 0–1 cm depth layer to 1.4×10^7 cells g^{-1} in the 5–10 cm depth layer in the abyssal west Pacific. In the eastern CCZ, bacterial biomasses range from 238 mg C m^{-2} to 530 mg C m^{-2} (Pape et al., 2017; Sweetman et al., 2019) in the upper 5 cm of sediment which will be removed during industrial deep-seabed mining operations. As the models presented here indicate, the microbial loop in the upper 5 cm of sediment contributes between 70% and 71% to T_r at the GSR exploration license area. Hence, we can expect that an impairment of the microbial loop during deep-seabed mining operations will have the largest impact on benthic carbon cycling. Vonnahme et al. (2020) measured an up to fourfold lower prokaryotic activity in a 5-week-old epibenthic sledge track in the more eutrophic (compared to the CCZ) abyssal Peru Basin. Assuming that sediment removal by mining will have a similar, if not stronger effect on the microbial loop in the CCZ, benthic carbon cycling at the GSR exploration license area will be further reduced by 0.63 $\text{mmol C m}^{-2} \text{d}^{-1}$. Hence, this study indicates that deep-seabed mining in the GSR license area will likely reduce ecosystem function in the form of carbon cycling by minimum 57 to 61% on a millennial timescale (Volz et al., 2020). Further expected loss of nodule-independent metazoan meiobenthos, macrobenthos, and other invertebrate megabenthos has not been taken into account.

5 Conclusion

Based on very highly resolved abyssal food-web models for two sites in the GSR exploration license area, I show that benthic carbon cycling in the eastern CCZ varies regionally (280 km) on the same order of magnitude as benthic carbon cycling 26 years after a small-scale sediment disturbance experiment between reference sites and areas likely affected by re-sedimentation (i.e., sites called ‘outside the plough tracks’ in de Jonge et al. (2020)). Hence, the International Seabed Authority should request a spatially (and temporally) very homogenous and fine-scale (environmental baseline) sample coverage for each sub-exploration license area in the CCZ in order to assess serious harm to the marine environment (Levin et al., 2016) and to determine potential recovery from subsequent

deep-seabed mining later on. The models furthermore indicate that polymetallic nodule-dependent fauna has a very minor contribution to benthic carbon cycling, though it is important for marine biodiversity (Niner et al., 2018; Stratmann et al., 2021) and therefore the author recommends concentrating on the microbial loop when investigating whether this specific ecosystem function is affected by deep-seabed mining as well as on biodiversity.

Data availability statement

The original contributions presented in the study are included in the article/Supplementary Material. Further inquiries can be directed to the corresponding author.

Author contributions

The author confirms being the sole contributor of this work and has approved it for publication.

Funding

This study received funding by JPI Oceans – Impacts of deep-sea nodule mining project “Mining Impact 2” from the Dutch Research council (NWO-ALW grant 856.18.003), from the research program NWO-Rubicon with project number 019.182EN.012, and from the NWO-Talent program Veni with project number VI.Veni.212.211.

Conflict of interest

The author declares that the research was conducted in the absence of any commercial or financial relationships that could be construed as a potential conflict of interest.

The handling editor MH declared a past collaboration with the author TS.

Publisher’s note

All claims expressed in this article are solely those of the authors and do not necessarily represent those of their affiliated organizations, or those of the publisher, the editors and the reviewers. Any product that may be evaluated in this article, or claim that may be made by its manufacturer, is not guaranteed or endorsed by the publisher.

Supplementary material

The Supplementary Material for this article can be found online at: <https://www.frontiersin.org/articles/10.3389/fmars.2023.1151442/full#supplementary-material>

References

- Bligh, E. G., and Dyer, W. J. (1959). A rapid method of total lipid extraction and purification. *Can. J. Biochem. Physiol.* 37, 911–917. doi: 10.1139/o59-099
- Blöthe, M., Węgorzewski, A., Müller, C., Simon, F., Kuhn, T., and Schippers, A. (2015). Manganese-cycling microbial communities inside deep-sea manganese nodules. *Environ. Sci. Technol.* 49, 7692–7700. doi: 10.1021/es504930v
- Boschker, H. T. S., de Brouwer, J. F. C., and Cappenberg, T. E. (1999). The contribution of macrophyte-derived organic matter to microbial biomass in salt-marsh sediments: stable carbon isotope analysis of microbial biomarkers. *Limnol. Oceanogr.* 44, 309–319. doi: 10.4319/lo.1999.44.2.0309
- Brinch-Iversen, J., and King, G. M. (1990). Effects of substrate concentration, growth state, and oxygen availability on relationships among bacterial carbon, nitrogen and phospholipid phosphorus content. *FEMS Microbiol. Lett.* 74, 345–355. doi: 10.1111/j.1574-6968.1990.tb04081.x
- Cho, H., Kim, K. H., Son, S. K., and Hyun, J. H. (2018). Fine-scale microbial communities associated with manganese nodules in deep-sea sediment of the Korea deep ocean study area in the northeast equatorial pacific. *Ocean Sci. J.* 53, 337–353. doi: 10.1007/s12601-018-0032-0
- Clausen, I., and Riisgård, H. U. (1996). Growth, filtration and respiration in the mussel *mytilus edulis*: no evidence for physiological regulation of the filter-pump to nutritional needs. *Mar. Ecol. Prog. Ser.* 141, 37–45. doi: 10.3354/meps141037
- Cormier, M.-H., and Sloan, H. (2018). “Abyssal hills and abyssal plains,” in *Submarine geomorphology springer geology*. Eds. A. Micallef, S. Krastel and A. Savini (Cham: Springer International Publishing), 389–408. doi: 10.1007/978-3-319-57852-1
- Crisp, D. (1971). “Energy flow measurements,” in *Methods for the study of marine benthos*. Eds. N. A. Holme and A. D. McIntyre (Oxford: Blackwell Scientific Publications), 284–367.
- Danovaro, R., Dell’Anno, A., Corinaldesi, C., Magagnoli, M., Noble, R., Tamburini, C., et al. (2008). Major viral impact on the functioning of benthic deep-sea ecosystems. *Nature* 454, 1084–1087. doi: 10.1038/nature07268
- de Jonge, V. N. (1980). Fluctuations in the organic carbon to chlorophyll a ratios for estuarine benthic diatom populations. *Mar. Ecol. Prog. Ser.* 2, 345–353. doi: 10.3354/meps002345
- de Jonge, D. S. W., Stratmann, T., Lins, L., Vanreusel, A., Purser, A., Marcon, Y., et al. (2020). Abyssal food-web model indicates faunal carbon flow recovery and impaired microbial loop 26 years after a sediment disturbance experiment. *Prog. Oceanogr.* 189, 102446. doi: 10.1016/j.pocan.2020.102446
- de Smet, B., Pape, E., Riehl, T., Bonifácio, P., Colson, L., and Vanreusel, A. (2017). The community structure of deep-sea macrofauna associated with polymetallic nodules in the eastern part of the clarion-clipperton fracture zone. *Front. Mar. Sci.* 4. doi: 10.3389/fmars.2017.00103
- de Smet, B., Simon-Lledó, E., Mevenkamp, L., Pape, E., Pasotti, F., Jones, D. O. B., et al. (2021). The megafauna community from an abyssal area of interest for mining of polymetallic nodules. *Deep-Sea Res. I* 172, 103530.
- de Smet, B., van Oevelen, D., Vincx, M., Vanaverbeke, J., and Soetaert, K. (2016). Lanice conchilega structures carbon flows in soft-bottom intertidal areas. *Mar. Ecol. Prog. Ser.* 552, 47–60. doi: 10.3354/meps11747
- Drazen, J. C., Leitner, A. B., Jones, D. O. B., and Simon-Lledó, E. (2021). Regional variation in communities of demersal fishes and scavengers across the CCZ and pacific ocean. *Front. Mar. Sci.* 8. doi: 10.3389/fmars.2021.630616
- Drazen, J. C., and Seibel, B. A. (2007). Depth-related trends in metabolism of benthic and benthopelagic deep-sea fishes. *Limnol. Oceanogr.* 52, 2306–2316. doi: 10.4319/lo.2007.52.5.2306
- Drazen, J. C., and Yeh, J. (2012). Respiration of four species of deep-sea demersal fishes measured *in situ* in the eastern north pacific. *Deep-Sea Res. I* 60, 1–6. doi: 10.1016/j.dsr.2011.09.007
- Dunlop, K. M., van Oevelen, D., Ruhl, H. A., Huffard, C. L., Kuhn, L. A., and Smith, K. L. (2016). Carbon cycling in the deep eastern north pacific benthic food web: investigating the effect of organic carbon input. *Limnol. Oceanogr.* 61, 1956–1968. doi: 10.1002/lno.10345
- Durden, J. M., Ruhl, H. A., Pebody, C. A., Blackbird, S. J., and van Oevelen, D. (2017). Differences in the carbon flows in the benthic food webs of abyssal hill and plain habitats. *Limnol. Oceanogr.* 62, 1771–1782. doi: 10.1002/lno.10532
- Fabiano, M., Danovaro, R., and Fraschetti, S. (1995). A three-year time series of elemental and biochemical composition of organic matter in subtidal sandy sediments of the ligurian Sea (northwestern Mediterranean). *Cont. Shelf Res.* 15, 1453–1469. doi: 10.1016/0278-4343(94)00088-5
- Gage, J. D., and Tyler, P. A. (1991). *Deep-sea biology: a natural history of organisms at the deep-sea floor* (Cambridge, UK: Cambridge University Press).
- Glover, A. G., Dahlgren, T., Wiklund, H., Mohrbeck, I., and Smith, C. (2015). An end-to-end DNA taxonomy methodology for benthic biodiversity survey in the clarion-clipperton zone, central pacific abyss. *J. Mar. Sci. Eng.* 4, 2. doi: 10.3390/jmse4010002
- Goineau, A., and Gooday, A. J. (2017). Novel benthic foraminifera are abundant and diverse in an area of the abyssal equatorial pacific licensed for polymetallic nodule exploration. *Sci. Rep.* 7, 45288. doi: 10.1038/srep45288
- Gooday, A. J., and Goineau, A. (2019). The contribution of fine sieve fractions (63–150 μm) to foraminiferal abundance and diversity in an area of the eastern pacific ocean licensed for polymetallic nodule exploration. *Front. Mar. Sci.* 6. doi: 10.3389/fmars.2019.00114
- Gooday, A. J., Goineau, A., and Voltski, I. (2015). Abyssal foraminifera attached to polymetallic nodules from the eastern clarion-clipperton fracture zone: a preliminary description and comparison with north Atlantic dropstone assemblages. *Mar. Biodiversity* 45, 391–412. doi: 10.1007/s12526-014-0301-9
- Gooday, A. J., Holzmann, M., Caille, C., Goineau, A., Kamenskaya, O., Weber, A. A. T., et al. (2017). Giant protists (Xenophyophores, foraminifera) are exceptionally diverse in parts of the abyssal eastern pacific licensed for polymetallic nodule exploration. *Biol. Conserv.* 207, 106–116. doi: 10.1016/j.biocon.2017.01.006
- Gooday, A. J., Lejzerowicz, F., Goineau, A., Holzmann, M., Kamenskaya, O., Kitazato, H., et al. (2021). The biodiversity and distribution of abyssal benthic foraminifera and their possible ecological roles: a synthesis across the clarion-clipperton zone. *Front. Mar. Sci.* 8. doi: 10.3389/fmars.2021.634726
- Gooday, A. J., Schoenle, A., Dolan, J. R., and Arndt, H. (2020). Protist diversity and function in the dark ocean – challenging the paradigms of deep-sea ecology with special emphasis on foraminiferans and naked protists. *Eur. J. Protistol.* 75, 125721. doi: 10.1016/j.ejop.2020.125721
- Gooday, A. J., and Wawrzyniak-Wydrowska, B. (2023). Macrofauna-sized foraminifera in epibenthic sledge samples from five areas in the eastern clarion-clipperton zone (equatorial pacific). *Front. Mar. Sci.* 9. doi: 10.3389/fmars.2022.1059616
- Harbour, R. P., Leitner, A. B., Rühlemann, C., Vink, A., and Sweetman, A. K. (2020). Benthic and demersal scavenger biodiversity in the eastern end of the clarion-clipperton zone – an area marked for polymetallic nodule mining. *Front. Mar. Sci.* 7. doi: 10.3389/fmars.2020.00458
- Harris, P. T., Macmillan-Lawler, M., Rupp, J., and Baker, E. K. (2014). Geomorphology of the oceans. *Mar. Geol.* 352, 4–24. doi: 10.1016/j.margeo.2014.01.011
- Hauquier, F., Macheriotou, L., Bezerra, T. N., Egho, G., Martínez Arbizu, P., and Vanreusel, A. (2019). Distribution of free-living marine nematodes in the clarion-clipperton zone: implications for future deep-sea mining scenarios. *Biogeosciences* 16, 3475–3489. doi: 10.5194/bg-16-3475-2019
- Hauton, C., Brown, A., Thatje, S., Mestre, N. C., Bebianno, M. J., Martins, I., et al. (2017). Identifying toxic impacts of metals potentially released during deep-sea mining – a synthesis of the challenges to quantifying risk. *Front. Mar. Sci.* 4. doi: 10.3389/fmars.2017.00368
- Hein, J. R., and Koschinsky, A. (2014). “Deep-ocean ferromanganese crusts and nodules,” in *Treatise on geochemistry*. Eds. H. Holland and K. Turekian (Amsterdam: Elsevier Ltd), 273–291. doi: 10.1016/B978-0-08-095975-7.01111-6
- Hein, J. R., Mizell, K., Koschinsky, A., and Conrad, T. A. (2013). Deep-ocean mineral deposits as a source of critical metals for high- and green-technology applications: comparison with land-based resources. *Ore Geol. Rev.* 51, 1–14. doi: 10.1016/j.joregeorev.2012.12.001
- Hoving, H.-J., Boetius, A., Dunlop, K., Greinert, J., Haeckel, M., Jones, D. O. B., et al. Major fine-scale spatial heterogeneity in an accumulation of gelatinous carbon fluxes on the deep seabed. *Frontiers in Marine Science*.
- Hughes, J. A., and Gooday, A. J. (2004). Associations between living benthic foraminifera and dead tests of *syringammina fragilissima* (Xenophyophorea) in the Darwin mounds region (NE Atlantic). *Deep Sea Res. I Oceanogr. Res. Pap.* 51, 1741–1758. doi: 10.1016/j.dsr.2004.06.004
- International Seabed Authority (2011). *Draft environmental management plan for the clarion-clipperton zone I* (Kingston, Jamaica: International Seabed Authority).
- Jørgensen, B. B., and Boetius, A. (2007). Feast and famine [amp]mdash; microbial life in the deep-sea bed. *Nat. Rev. Microbiol.* 5, 770–781. doi: 10.1038/nrmicro1745
- Jumars, P. A., Dorgan, K. M., and Lindsay, S. M. (2015). Diet of worms emended: an update of polychaete feeding guilds. *Ann. Rev. Mar. Sci.* 7, 497–520. doi: 10.1146/annurev-marine-010814-020007
- Kersken, D., Janussen, D., and Martínez Arbizu, P. (2018). Deep-sea glass sponges (Hexactinellida) from polymetallic nodule fields in the clarion-clipperton fracture zone (CCFZ), northeastern pacific: part I – amphidiscophora. *Mar. Biodiversity* 48, 545–573. doi: 10.1007/s12526-017-0727-y
- Kones, J. K., Soetaert, K., van Oevelen, D., and Owino, J. O. (2009). Are network indices robust indicators of food web functioning? a Monte Carlo approach. *Ecol. Modell.* 220, 370–382. doi: 10.1016/j.ecolmodel.2008.10.012
- Koschinsky, A., Gaye-Haake, B., Arndt, C., Maue, G., Spitz, A., Winkler, A., et al. (2001). Experiments on the influence of sediment disturbances on the biogeochemistry of the deep-sea environment. *Deep-Sea Res. II* 48, 3629–3651. doi: 10.1016/S0967-0645(01)00060-1
- Kuhn, T., Węgorzewski, A. v., Rühlemann, C., and Vink, A. (2017). “Composition, formation, and occurrence of polymetallic nodules,” in *Deep-Sea mining*. Ed. R. Sharma (Cham: Springer International Publishing), 23–63. doi: 10.1007/978-3-319-52557-0_2
- Leitner, A. B., Drazen, J. C., and Smith, C. R. (2021). Testing the seamount refuge hypothesis for predators and scavengers in the Western clarion-clipperton zone. *Front. Mar. Sci.* 8. doi: 10.3389/fmars.2021.636305

- Leitner, A. B., Durden, J. M., Smith, C. R., Klingberg, E. D., and Drazen, J. C. (2020). Synaphobranchid eel swarms on abyssal seamounts: largest aggregation of fishes ever observed at abyssal depths. *Deep Sea Res. 1 Oceanogr Res. Pap* 167 103423. doi: 10.1016/j.dsr.2020.103423
- Levin, L. A., Mengerink, K. J., Gjerde, K. M., Rowden, A. A., van Dover, C. L., Clark, M. R., et al. (2016). Defining "serious harm" to the marine environment in the context of deep-seabed mining. *Mar. Policy* 74, 245–259. doi: 10.1016/j.marpol.2016.09.032
- Lim, S.-C., Wiklund, H., Glover, A. G., Dahlgren, T. G., and Tan, K.-S. (2017). A new genus and species of abyssal sponge commonly encrusting polymetallic nodules in the clarion-clipperton zone, East Pacific Ocean. *Syst. Biodivers* 15, 507–519. doi: 10.1080/14722000.2017.1358218
- McQuaid, K. A., Attrill, M. J., Clark, M. R., Cobley, A., Glover, A. G., Smith, C. R., et al. (2020). Using habitat classification to assess representativity of a protected area network in a large, data-poor area targeted for deep-sea mining. *Front. Mar. Sci.* 7. doi: 10.3389/fmars.2020.558860
- Menzies, R. J. (1962). On the food and feeding habits of abyssal organisms as exemplified by the isopoda. *Internationale Rev. der gesamten Hydrobiologie und Hydrographie* 47, 339–358. doi: 10.1002/iroh.19620470303
- Middelburg, J. J., Barranguet, C., Boschker, H. T. S., Herman, P. M. J., Moens, T., and Heip, C. H. R. (2000). The fate of intertidal microphytobenthos carbon: an *in situ* ¹³C-labeling study. *Limnol Oceanogr* 45, 1224–1234. doi: 10.4319/lo.2000.45.6.1224
- Miller, K. A., Thompson, K. F., Johnston, P., and Santillo, D. (2018). An overview of seabed mining including the current state of development, environmental impacts, and knowledge gaps. *Front. Mar. Sci.* 4. doi: 10.3389/fmars.2017.00418
- Molari, M., Janssen, F., Janssen, F., Vonnahme, T. R., Vonnahme, T. R., Wenzhöfer, F., et al. (2020). The contribution of microbial communities in polymetallic nodules to the diversity of the deep-sea microbiome of the Peru basin (4130–4198m depth). *Biogeosciences* 17, 3203–3222. doi: 10.5194/bg-17-3203-2020
- Mullineaux, L. S. (1987). Organisms living on manganese nodules and crusts: distribution and abundance at three north Pacific sites. *Deep-Sea Res.* 34, 165–184.
- Mullineaux, L. S. (1989). Vertical distribution of the epifauna on manganese nodules: implication for settlement and feeding. *Limnol Oceanogr* 34, 1247–1262.
- Niner, H. J., Ardron, J. A., Escobar Briones, E., Gianni, M., Jaekel, A., Jones, D. O. B., et al. (2018). Deep-sea mining with no net loss of biodiversity - an impossible aim. *Front. Mar. Sci.* 5. doi: 10.3389/fmars.2018.00053
- Nomaki, H., Rastelli, E., Alves, A., Suga, H., Ramos, S., Kitahashi, T., et al. (2021). Abyssal fauna, benthic microbes, and organic matter quality across a range of trophic conditions in the western Pacific Ocean. *Prog. Oceanogr* 195, 102591. doi: 10.1016/j.pocean.2021.102591
- Pape, E., Bezerra, T. N., Hauquier, F., and Vanreusel, A. (2017). Limited spatial and temporal variability in meiofauna and nematode communities at distant but environmentally similar sites in an area of interest for deep-sea mining. *Front. Mar. Sci.* 4. doi: 10.3389/fmars.2017.00205
- Pasotti, F., Mevenkamp, L., Pape, E., Blazewicz, M., Bonifácio, P., Riehl, T., et al. (2021). A local scale analysis of manganese nodules influence on the clarion-clipperton fracture zone macrobenthos. *Deep-Sea Res. I* 168, 103449. doi: 10.1016/j.dsr.2020.103449
- Petersen, S., Krätschell, A., Augustin, N., Jamieson, J., Hein, J. R., and Hannington, M. D. (2016). News from the seabed – geological characteristics and resource potential of deep-sea mineral resources. *Mar. Policy* 70, 175–187. doi: 10.1016/j.marpol.2016.03.012
- R-Core Team (2017) *R: a language and environment for statistical computing*. Available at: <https://www.r-project.org/>.
- Schoening, T., Purser, A., Langenkämper, D., Suck, I., Taylor, J., Cuvelier, D., et al. (2020). Megafauna community assessment of polymetallic-nodule fields with cameras: platform and methodology comparison. *Biogeosciences* 17, 3115–3133. doi: 10.5194/bg-17-3115-2020
- Simon-Lledó, E., Bett, B. J., Huvenne, V. A. I., Schoening, T., Benoist, N. M. A., Jeffreys, R. M., et al. (2019a). Megafaunal variation in the abyssal landscape of the clarion clipperton zone. *Prog. Oceanogr* 170, 119–133. doi: 10.1016/j.pocean.2018.11.003
- Simon-Lledó, E., Bett, B. J., Huvenne, V. A. I., Schoening, T., Benoist, N. M. A., and Jones, D. O. B. (2019b). Ecology of a polymetallic nodule occurrence gradient: implications for deep-sea mining. *Limnol Oceanogr* 64, 1883–1894. doi: 10.1002/lno.11157
- Simon-Lledó, E., Pomee, C., Ahokava, A., Drazen, J. C., Leitner, A. B., Flynn, A., et al. (2020). Multi-scale variations in invertebrate and fish megafauna in the mid-eastern clarion clipperton zone. *Prog. Oceanogr* 187, 102405. doi: 10.1016/j.pocean.2020.102405
- Smith, K. L. (1978). Metabolism of the abyssopelagic rattail *Coryphaenoides armatus* measured *in situ*. *Nature* 274, 362–364. doi: 10.1038/274362a0
- Smith, C. R., de Léo, F. C., Bernardino, A. F., Sweetman, A. K., and Martínez Arbizu, P. (2008). Abyssal food limitation, ecosystem structure and climate change. *Trends Ecol. Evol.* 23, 518–528. doi: 10.1016/j.tree.2008.05.002
- Smith, K. L., and Hessler, R. R. (1974). Respiration of benthopelagic fishes: *in situ* measurements at 1230 meters. *Science* 184, 72–73.
- Soetaert, K., and van Oevelen, D. (2009). Modeling food web interactions in benthic deep-sea ecosystems: a practical guide. *Oceanography* 22, 128–143. doi: 10.5670/oceanog.2009.13
- Stachowska-Kamińska, Z., Gooday, A. J., Radziejewska, T., and Arbizu, P. M. (2022). Macrofaunal foraminifera from a former benthic impact experiment site (IOM contract area) in the abyssal eastern clarion-clipperton zone 103848. *Deep Sea Res. 1 Oceanogr Res. Pap* 188. doi: 10.1016/j.dsr.2022.103848
- Stratmann, T., Lins, L., Purser, A., Marcon, Y., Rodrigues, C. F., Ravara, A., et al. (2018a). Abyssal plain faunal carbon flows remain depressed 26 years after a simulated deep-sea mining disturbance. *Biogeosciences* 15, 4131–4145. doi: 10.5194/bg-15-4131-2018
- Stratmann, T., Mevenkamp, L., Sweetman, A. K., Vanreusel, A., and van Oevelen, D. (2018b). Has phytodetritus processing by an abyssal soft-sediment community recovered 26 years after an experimental disturbance? *Front. Mar. Sci.* 5. doi: 10.3389/fmars.2018.00059
- Stratmann, T., Soetaert, K., Kersken, D., and Van Oevelen, D. (2021). Polymetallic nodules are essential for food-web integrity of a prospective deep-seabed mining area in Pacific abyssal plains. *Sci. Rep.* 11, 12238. doi: 10.1038/s41598-021-91703-4
- Sweetman, A. K., Smith, C. R., Shulze, C. N., Maillot, B., Lindh, M., Church, M. J., et al. (2019). Key role of bacteria in the short-term cycling of carbon at the abyssal seafloor in a low particulate organic carbon flux region of the eastern Pacific Ocean. *Limnol Oceanogr* 64, 694–713. doi: 10.1002/lno.11069
- Uhlenkott, K., Vink, A., Kuhn, T., Gillard, B., and Arbizu, P. M. (2021). Meiofauna in a potential deep-sea mining area: influence of temporal and spatial variability on small-scale abundance models. *Diversity (Basel)* 13, 3. doi: 10.3390/d13010003
- van Oevelen, D., Soetaert, K., and Heip, C. H. R. (2012). Carbon flows in the benthic food web of the porcupine abyssal plain: the (un)importance of labile detritus in supporting microbial and faunal carbon demands. *Limnol Oceanogr* 57, 645–664. doi: 10.4319/lo.2012.57.2.0645
- van Oevelen, D., van den Meersche, K., Meysman, F. J. R., Soetaert, K., Middelburg, J. J., and Vézina, A. F. (2010). Quantifying food web flows using linear inverse models. *Ecosystems* 13, 32–45. doi: 10.1007/s10021-009-9297-6
- Vanreusel, A., Hilário, A., Ribeiro, P. A., Menot, L., and Martínez Arbizu, P. (2016). Threatened by mining, polymetallic nodules are required to preserve abyssal epifauna. *Sci. Rep.* 6, 26808. doi: 10.1038/srep26808
- Veillette, J., Sarrazin, J., Gooday, A. J., Galéron, J., Caprais, J. C., Vangriesheim, A., et al. (2007). Ferromanganese nodule fauna in the tropical north Pacific Ocean: species richness, faunal cover and spatial distribution. *Deep-Sea Res. I* 54, 1912–1935. doi: 10.1016/j.dsr.2007.06.011
- Volz, J. B., Haffert, L., Haeckel, M., Koschinsky, A., and Kasten, S. (2020). Impact of small-scale disturbances on geochemical conditions, biogeochemical processes and element fluxes in surface sediments of the eastern clarion-clipperton zone, Pacific Ocean. *Biogeosciences* 17, 1113–1131. doi: 10.5194/bg-17-1113-2020
- Volz, J. B., Volz, J. B., Mogollón, J. M., Geibert, W., Martínez, P., Arbizu, P. M., et al. (2018). Natural spatial variability of depositional conditions, biogeochemical processes and element fluxes in sediments of the eastern clarion-clipperton zone, Pacific Ocean. *Deep-Sea Res. I* 140, 159–172. doi: 10.1016/j.dsr.2018.08.006
- Vonnahme, T. R., Molari, M., Janssen, F., Wenzhöfer, F., Haeckel, M., Titschack, J., et al. (2020). Effects of a deep-sea mining experiment on seafloor microbial communities and functions after 26 years. *Sci. Adv.* 6, eaaz5922. doi: 10.1126/sciadv.aaz5922
- Wang, X., Schröder, H. C., Wiens, M., Schloßmacher, U., and Müller, W. E. G. (2009). Manganese/polymetallic nodules: micro-structural characterization of exolithobiontic- and endolithobiontic microbial biofilms by scanning electron microscopy. *Micron* 40, 350–358. doi: 10.1016/j.micron.2008.10.005
- Washburn, T. W., Jones, D. O. B., Wei, C.-L., and Smith, C. R. (2021). Environmental heterogeneity throughout the clarion-clipperton zone and the potential representativity of the APEI network. *Front. Mar. Sci.* 8. doi: 10.3389/fmars.2021.661685
- Wieser, W. (1953). Die Beziehung zwischen mundhöhlengestalt, ernährungsweise und vorkommen bei freilebenden marinen nematoden. *Arkiv för Zoologie* 4, 439–484.
- Witte, U., Wenzhöfer, F., Sommer, S., Boetius, A., Heinz, P., Aberle, N., et al. (2003). *In situ* experimental evidence of the fate of a phytodetritus pulse at the abyssal sea floor. *Nature* 424, 763–766. doi: 10.1038/nature01799